Meteorol. Zeitschrift, N.F. 1, 87—121 (April 1992)

A thermodynamic diagnostic model for the atmosphere. Part I: Analysis of the August 1991 rain episode in Austria

M. DORNINGER, M. EHRENDORFER, M. HANTEL, F. RUBEL and Y. WANG, Wien

Summary. A diagnostic model (acronym DIAMOD) for the free atmosphere is described. Core of DIAMOD is a module which calculates complete thermodynamic budgets of latent and sensible heat, including objective imbalance estimates. Input data are the uninitialized ECMWF analyses and the objectively analysed SYNOP precipitation field; these are specified on the gridscale (horizontal/vertical/time boxes of dimensions 100 km/100 hPa/12 h). Main output quantities are vertical profiles of the sub-gridscale fluxes of rain and of moisture and heat ($\overline{q'\omega'}$, $\overline{T'\omega'}$); their divergences represent important components of the thermodynamic budgets.

DIAMOD is applied to the intense Central European rain episode of August 1991 with maximum over northern Austria. The three sub-gridscale fluxes are the main diagnostic parameters considered, together with the analysed gridscale quantities. The column over Salzburg is discussed in detail. All sub-gridscale fluxes peak on 1 August 1991 with the rain flux exceeding 1600 W/m². The Salzburg column is unique in that all gridscale components (tendency, horizontal and vertical moisture flux convergence) plus the sub-gridscale moisture flux convergence have the same sign which maximizes the rain flux. It is demonstrated that, with DIAMOD, one can diagnostically distinguish between large-scale rain, convective rain and convection without rain. The rms-imbalance of all boxes over Europe is of the order of 50 W/m².

The theoretical background of DIAMOD will be discussed in Part II of this paper.

Ein thermodynamisches diagnostisches Modell für die Atmosphäre.
Teil I: Die Regenepisode in Österreich von August 1991

Zusammenfassung. Ein diagnostisches Modell (Akronym DIAMOD) für die freie Atmosphäre wird beschrieben. Zentraler Bestandteil von DIAMOD ist ein Modul zur Berechnung vollständiger thermodynamischer Budgets von latenter und fühlbarer Wärme, unter zusätzlicher Angabe objektiv geschätzter Imbalanzen. Eingangsgrößen sind die nicht-initialisierten Analysen des EZMW und das objektiv analysierte SYNOP Niederschlagsfeld; diese Felder werden auf der Gitterskala spezifiziert (horizontale/vertikale/zeitliche Boxen der Dimensionen 100 km/100 hPa/12 h). Die zentralen Ergebnisse sind die vertikalen Profile der subskaligen Flüsse von Regen und von Feuchte und Wärme ($\overline{q'\omega'}$, $\overline{T'\omega'}$); ihre Divergenzen stellen wichtige Bestandteile der thermodynamischen Budgets dar.

DIAMOD wird zur Untersuchung der Starkregenepisode Anfang August 1991 über Mitteleuropa herangezogen, deren Maximum über den nördlichen Teilen Österreichs auftrat. Die drei subskaligen Flüsse, sowie die analysierten gitterskaligen Größen sind die wesentlichen diagnostischen Parameter, die betrachtet werden. Die Säule über Salzburg wird ausführlich besprochen. Alle subskaligen Flüsse erreichen ihr Maximum am 1. August 1991, wobei der Regenfluß größer als 1600 W/m² ist. Die Säule über Salzburg ist einzigartig darin, daß alle gitterskaligen Komponenten (Tendenz, horizontale und vertikale Feuchteflußkonvergenz), sowie die subskalige Feuchteflußkonvergenz dasselbe Vorzeichen haben und somit zu einem Maximum des Regenflusses führen. Es wird gezeigt, daß es mit DIAMOD möglich ist, diagnostisch zwischen skaligem Regen, konvektivem Regen und Konvektion ohne Regen zu unterscheiden. Die rms-Imbalanz aller Boxen über Europa ist ungefähr 50 W/m².

Theoretische Details von DIAMOD werden in Teil II dieser Arbeit diskutiert.

1. Introduction

Torrential rains fell over Central Europe in the first days of August 1991. They caused widespread flooding with catastrophic conditions in some parts of Austria. The Austrian federal country Salzburg experienced a total rainfall of 85 mm per 3 days (1—3 August) with a maximum intensity of 28 mm per 12 hours. These figures are representative for an area of (100 km)² with Salzburg at about the center; local raingauge intensities were higher. The city of Salzburg recorded 230 mm per 4 days (30 July to 2 August), Salzburg Airport 71 mm per 12 hours (representative for 1 to 2 August) and the slopes of the Gaisberg (a mountain peak close to Salzburg with 1000 m summit) 346 mm per 3 days. On 1 August (Fig. 1.1) the rain maximum was located over southeastern Bavaria (Germany); on 2 August, it was located over Bohemia (Czechoslovakia) and, on 3 August, over Styria (Austria). The net precipitation over the entire episode peaked over Austria; a time series for the Salzburg region is shown in Fig. 1.2. The statistical return period of this event is (locally dependent) between 30 and 100 years.

It is the purpose of this paper to investigate the thermodynamic conditions that prevailed in the atmosphere over Europe during this period. We shall use the diagnostic model DIAMOD which has recently been implemented at the University of Vienna. Theory and applications of this model have in various preliminary forms been discussed by HANTEL (1982), EMEIS & HANTEL (1984), HANTEL et al. (1984), EMEIS (1985a), HANTEL (1987, 1989) and BURKHARDT (1991). The basic theoretical concept of DIAMOD is that in the thermodynamic budget equations for latent and sensible heat the three-dimensional (3D) gridscale terms (which together comprise the so-called budget) are specified from observations as routinely analysed fields provided by the European Centre for Medium-Range Weather Forecasts (ECMWF). Further specified are the energy fluxes across the earth's surface, notably precipitation (analysed SYNOP-fields). This allows to calculate an error estimate in each box in the vertical (the so-called *imbalance*). In a next step the energy equations are algebraically solved for the so-called *signal* which represents the residual of the

0941-2948/92/0001-0087 $ 15.75

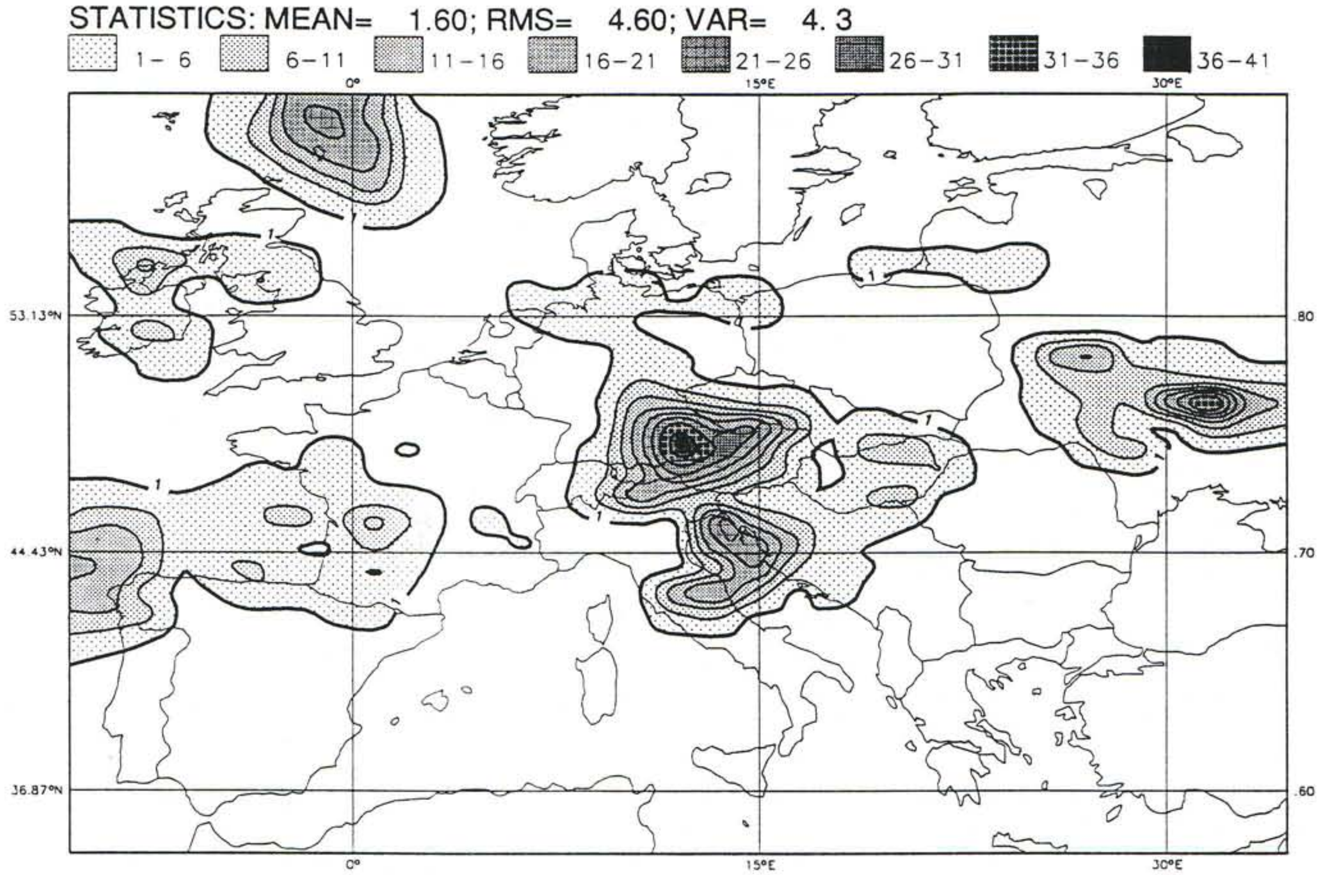

Fig. 1.1. Analysed surface precipitation over Europe in units mm/12h; precipitation measured at 1 August 1991, 06GMT; reported through SYNOP-network and objectively analysed on diagnostic grid with CRESSMANN method; contour interval 5 mm/12h; isoline 1 mm/12h bold; main maxima 38 mm/12h over SE-Bavaria and 35 mm/12h over Ukraine.

Abb. 1.1. Bodenniederschlag über Europa in mm/12h; gemessen am 1. August 1991, 06GMT; erhoben durch das SYNOP-Meßnetz und objektiv mittels CRESSMANN-Methode auf das Diagnosegitter analysiert; Konturintervall 5 mm/12h; 1 mm/12h-Isolinie dick; Hauptmaxima 35 mm/12h über Südost-Bayern und 35 mm/12h über der Ukraine.

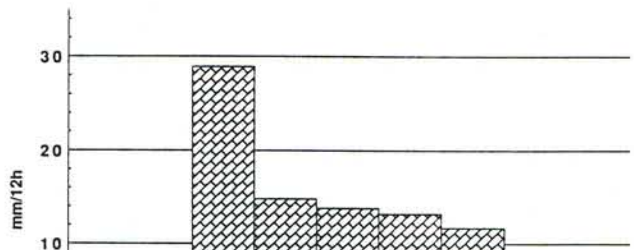

Fig. 1.2. Time series of surface precipitation over the SALZBURG column in units mm/12h from 31 July, 18GMT to 3 August, 18GMT; precipitation is representative for an area of (100 km)^2.

Abb. 1.2. Zeitserie des Bodenniederschlages der Säule SALZBURG in mm/12h vom 31. Juli, 18 GMT bis 3. August, 18GMT; Niederschlag ist repräsentativ für eine Fläche von (100 km)^2.

respective energy equation. Budget plus signal plus imbalance now equal zero in every atmospheric box in the vertical. The final step is to interprete the signal as consisting of the divergence of the vertical sub-gridscale flux of latent or sensible heat plus or minus the vertical precipitation flux divergence, depending upon the respective energy equation.

The three sub-gridscale fluxes are:

Rain flux $$L\bar{P} = r(p) \qquad (1.1)$$

Moisture flux $$g^{-1}L\overline{q'\omega'} = f(p) \qquad (1.2)$$

Heat flux $$g^{-1}c_p\overline{T'\omega'} = w(p) \qquad (1.3)$$

L is the condensation heat (assumed constant), g the earth's acceleration, and c_p the specific heat at constant pressure. $\bar{P}$ is the vertical precipitation flux in units kg $m^{-2}s^{-1}$. The overbar refers to an average over both the representative time interval and the horizontal area of the column considered. Since the individual contributions to $\bar{P}$ as well as to $\overline{q'\omega'}$ and $\overline{T'\omega'}$ are on scales far below the grid resolution of routinely analysed fields it is consistent to refer to r, f and w as *sub-gridscale* or eddy fluxes. This includes the rain flux and is despite the fact that all three are diagnosed on the gridscale. All three fluxes are positive downward and are presented and discussed in the energy unit W/m^2 throughout this paper. Further, r, f and w are functions of pressure within a given vertical column. In order to solve for these three unknowns from just two signals, an independent condition is required. We employ as simple closure assumption a generalized inverse Bowen ratio the vertical profile of which in the free atmosphere is specified *a priori* (HANTEL 1982); for further discussion of this point see Section 2 below and Part II of this paper (HANTEL et al. 1992).

The sub-gridscale vertical fluxes are far from being negligible. The divergences of r, f and w in vertical direction are indispensable components of the thermodynamic budgets. The corresponding mathematical task is to solve a linear integral-differential equation which eventually yields the vertical profiles r(p), f(p) and w(p). While the boundary conditions of the sub-gridscale fluxes have been observationally specified, their vertical profiles are controlled by the free atmosphere budgets. The sum of the two sub-gridscale fluxes of moisture and heat, $f + w = h$, shall be referred to as the *total convective heat flux.*

There seems to be a certain arbitrariness in our convention to speak of the rain flux as of a sub-gridscale quantity because it has become common practice in forecasting to distinguish between *large-scale precipitation* and *small-scale precipitation.* Large-scale seems to imply that this precipitation is resolved by the model (and thus must be a gridscale phenomenon) while small-scale precipitation is attributed to eddies (and thus must be sub-gridscale or convective). A forecast model parameterizes both rain types independently and thus can distinguish between them.

DIAMOD yields just one precipitation. It is calculated on the diagnostic grid, influences the gridscale budget and thus has the character of a gridscale signal; on the other hand, precipitation is made up by individual condensed particles the size of which is far below any resolvable scale and therefore cannot be anything but sub-gridscale. From this consideration it appears an academic dispute if the total rain r diagnosed by DIAMOD is to be interpreted large-scale or small-scale in the sense familiar to the forecast models. We shall maintain to refer to r as sub-gridscale, like we do for the sub-gridscale fluxes f and w.

We shall, however, distinguish between precipitation accompanied by a sizeable upward total convective heat flux h (this we shall label *convective*) and a precipitation accompanied by vanishing h (this we shall label *non-convective*). Obviously, there is a gradual transition between these extremes. The diagnostic model offers, by means of h, a quantitative measure of the convectiveness of a precipitation event.

Thus, in the thermodynamic budgets to be considered we shall have gridscale (or analysed) quantities which are the input parameters. From these we determine, as residuals, the divergences of the fluxes r(p), f(p) and w(p) as output from DIAMOD. The latter two, moisture flux and heat flux, are always interpreted convective. The rain flux r, on the other hand, can be interpreted convective or non-convective depending upon the relative size of h in the column. The three fluxes r, f and w together will be referred to as sub-gridscale, mainly in order to distinguish them from the gridscale input quantities.

Once the sub-gridscale fluxes have been determined, the budgets are complete. It then is a matter of personal preoccupation in terms of which budget components (gridscale or sub-gridscale) one wants to discuss the characteristics of the atmosphere during a given synoptic situation. In this paper we put most emphasis upon the sub-gridscale fluxes because these quantities indicate whether the grid precipitation is convective or non-convective.

This concept of diagnosing eddy fluxes from a gridscale budget has much in common with the familiar approach of YANAI et al. (1973) and others. Like YANAI it simultaneously evaluates the budgets of latent and sensible heat. However, instead of modeling a cloud ensemble we simply couple latent and sensible heat equation by specifying the vertical profile of a generalized inverse Bowen ratio. A further difference of our approach to practically all other budget models is that DIAMOD employs more observed/analysed input data than necessary. This redundancy yields an additional statement for the column imbalance which allows for an objective separation between signal and error.

In the present Part I we shall summarize the specific implementation of DIAMOD for a continental region consisting of an array of 32 × 32 columns with Austria in the center (Section 2). In Section 3 the input data are exemplified in terms of the synoptic situation of the first days of August 1991. Core of this study then is the detailed investigation of the atmospheric conditions during this intense rain episode. The vertical sub-gridscale fluxes of rain, moisture and heat are the prominent diagnostic parameters considered. We start with the SALZBURG column (Section 4) and proceed with describing the sub-gridscale flux fields over Central Europe (Section 5). The physical mechanisms that emerge from the objective technique of DIAMOD are, in a preliminary manner, discussed in Section 6 by means of selected examples. Some conclusions are discussed in Section 7.

2. The diagnostic model DIAMOD

This section is devoted to a detailed description of the diagnostic model DIAMOD that is used to investigate the thermodynamic conditions during the first days of August 1991. In its essence this model is based on the conservation or budget equations for moisture (latent heat), heat (dry enthalpy or sensible heat) and mass. A preliminary summary of the approach has been given by HANTEL (1987). In this paper the theoretical treatment of the model is limited to stating the governing equations and giving details of the implementation. A more in-depth discussion of the theoretical background will be presented in Part II of this study (HANTEL et al. 1992).

2.1 *Basic equations of DIAMOD*

The governing equations of the diagnostic model DIAMOD are written in the following form:

$$\underbrace{L\frac{\partial q}{\partial t} + L\nabla\cdot qV + L\frac{\partial q\omega}{\partial p}}_{b_q} + g\,\underbrace{\frac{\partial}{\partial p}\frac{1}{g}L\overline{q'\omega'}}_{f} + g\frac{\partial}{\partial p}\underbrace{L\bar{P}}_{r} + \mathrm{imb}_q = 0, \qquad (2.1)$$

$$\underbrace{c_p\frac{\partial T}{\partial t} + c_p\nabla\cdot TV + c_p\left(\frac{\partial}{\partial p} - \frac{\kappa}{p}\right)T\omega + g\frac{\partial R}{\partial p}}_{b_T} + g\left(\frac{\partial}{\partial p} - \frac{\kappa}{p}\right)\underbrace{\frac{1}{g}c_p\overline{T'\omega'}}_{w} - g\frac{\partial}{\partial p}\underbrace{L\bar{P}}_{r} + \mathrm{imb}_T = 0, \qquad (2.2)$$

$$\nabla\cdot V + \frac{\partial\omega}{\partial p} = 0. \qquad (2.3)$$

These equations represent conservation or budget equations for moisture (2.1), heat (2.2) and mass (2.3) using pressure p as vertical coordinate. The dimension of the terms in both eqs. (2.1) and (2.2) is W/kg, whereas the dimension of the mass conservation equation is s^{-1}. The meaning of most symbols is standard; L ($= 2.5\cdot 10^6$ J/kg), g ($= 9.8$ m/s^2), and c_p ($= 1004$ J$kg^{-1}K^{-1}$) as well as $\bar{P}$ have been introduced in Section 1; R is the net radiative flux in units of W/m^2; consistent with the sign of the vertical velocity ω both fluxes are taken positive if they are downward. The symbol **V** denotes the horizontal velocity vector; κ is the ratio of the gas constant for dry air to c_p and is taken here equal to 2/7.

Eq. (2.1) is derived by considering the conservation law of moisture (specific humidity q) with the source/sink terms expressed solely through the divergence of the precipitation flux. Eq. (2.2) represents a statement of the first law of thermodynamics with the same source/sink term as in (2.1) but with opposite sign and an additional diabatic heating term due to radiation. The total derivatives in both equations have been expanded and the continuity equation (2.3) has been used to express advection in the flux form. Subsequent averaging of the equations over appropriate time and space intervals generates the terms $\overline{q'\omega'}$ and $\overline{T'\omega'}$. Since the averaging has already been carried out in eqs. (2.1)—(2.3) the symbols q, T, **V** and ω (and also R) [without an overbar] represent values of these variables for the averaging interval. Included in both eqs. (2.1) and (2.2) are imbalance terms to account for data inadequacies and/or model deficiencies. No imbalance term is included in the mass conservation equation, since the wind field considered is exactly satisfying (2.3) after appropriate modification (see Section 2.2).

With the abbreviations indicated in eqs. (2.1) and (2.2) the diagnostic approach of this study is as follows: the *gridscale* moisture and temperature budgets b_q and b_T specified from observations are balanced by divergences of the *sub-gridscale* rain, moisture and heat fluxes (r, f and w, respectively; unit W/m^2; positive downward). [Note that radiative processes are included in b_T.] These fluxes are essential in closing the budget equations; the gridscale budget terms (specified from observations) carry the information to infer the sub-gridscale processes. It is clear that this inference depends crucially on the quality of the gridscale diagnosis of the atmosphere.

2.2 *Implementation of DIAMOD*

For the actual investigation of the sub-gridscale processes appearing in the above equations the specific implementation of DIAMOD described in this subsection is used (see also Fig. 2.1).

In this implementation the budget equations (2.1)—(2.3) are discretized in a volume integration approach by considering columns of equal mass extending throughout the atmosphere. These columns have equal mass due to the choice of pressure as vertical coordinate and due to the choice of the horizontal coordinates that are taken as geographic longitude λ (positive eastward) and μ as the sine of geographic latitude ϕ (positive northward). The horizontal resolution of the *elementary grid* is approximately 50 km with a vertical resolution of 50 hPa (the surface pressure p_s is uniformly taken as $p_s = 1000$ hPa). A schematic of the resulting *elementary box* is shown in Fig. 2.2.

Starting with observations of the gridscale quantities q, T, **V** and ω available on the elementary grid every six hours (see Section 3), the moisture and temperature budgets b_q and b_T are computed by numerical integration of eqs. (2.1) and (2.2) over space and time. The space integration is extended over the mass of a *diagnostic box* that consists of eight elementary boxes (see Fig. 2.2) resulting in a transformation of most terms into differences of fluxes across the faces of the box; only the energy conversion term $\frac{\kappa}{p}T\omega$ requires a numerical volume integration. The time integration is performed over 12 hours using Simpson's rule. As indicated in Fig. 2.1, this process — described in more detail by SPANGL (1991) — results in gridscale budgets of moisture and heat for each box of the *diagnostic grid*. The diagnostic grid consists of 32×32 columns each having 10 diagnostic boxes in the vertical (see Fig. 2.3).

In the process of the numerical computation of b_q and b_T through differences of fluxes it is of utmost importance to employ a wind field that is exactly satisfying the discretized form of the continuity equation (2.3), since even extremely small noise divergences in the mass field make further budget considerations meaningless. For this purpose, the noise divergence of the wind field is removed by a variational procedure suggested by HANTEL (1986a). This modification requires the solution of a three-dimensional Poisson equation (see Fig. 2.1) which is implemented in

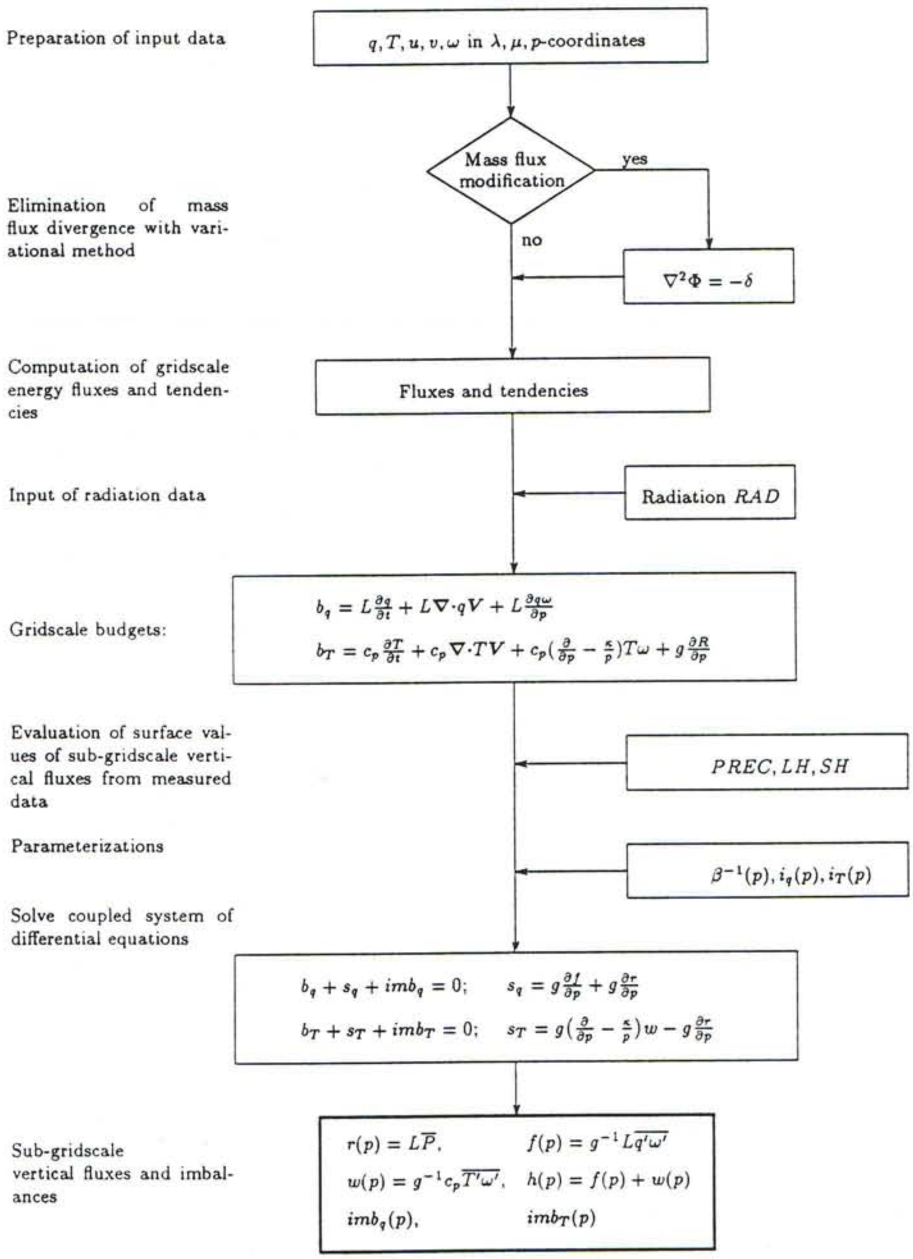

Fig. 2.1. Principal flow diagram of DIAMOD; further discussion see text.

Abb. 2.1. Prinzipielles Flußdiagramm von DIAMOD; zur Erklärung siehe Text.

DIAMOD by a fast, direct algorithm described by WANG et al. (1992) (see also Section 3.1).

In order to extract the vertical structure of the sub-gridscale *signal* (i.e., the fluxes r, f and w) from eqs. (2.1) and (2.2) it is necessary to introduce several approximations and assumptions into DIAMOD that are summarized in the following. A more detailed outline is given by DORNINGER (1992).

The first step in this context consists of an integration of eqs. (2.1) and (2.2) throughout the atmosphere. We assume that the fluxes r, f and w are available at the surface ($p = p_s$) from observations. In addition, these fluxes vanish at the top of the atmosphere ($p = 0$). Therefore, the vertically averaged moisture equation

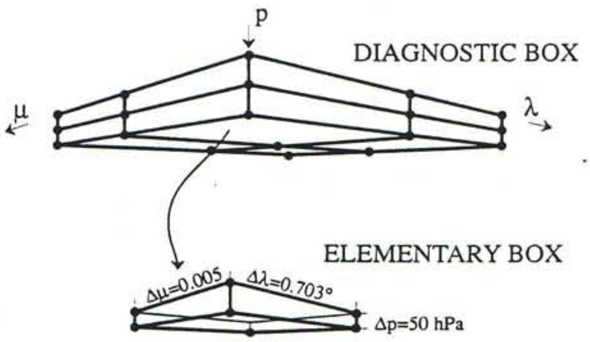

Fig. 2.2. Sketch of grids used; resolution indicated for elementary grid; each diagnostic column based on an area of (100 km)².

Abb. 2.2. Skizze des verwendeten Gitters; Auflösung des Elementargitters angegeben; Grundfläche jeder diagnostischen Säule beträgt (100 km)².

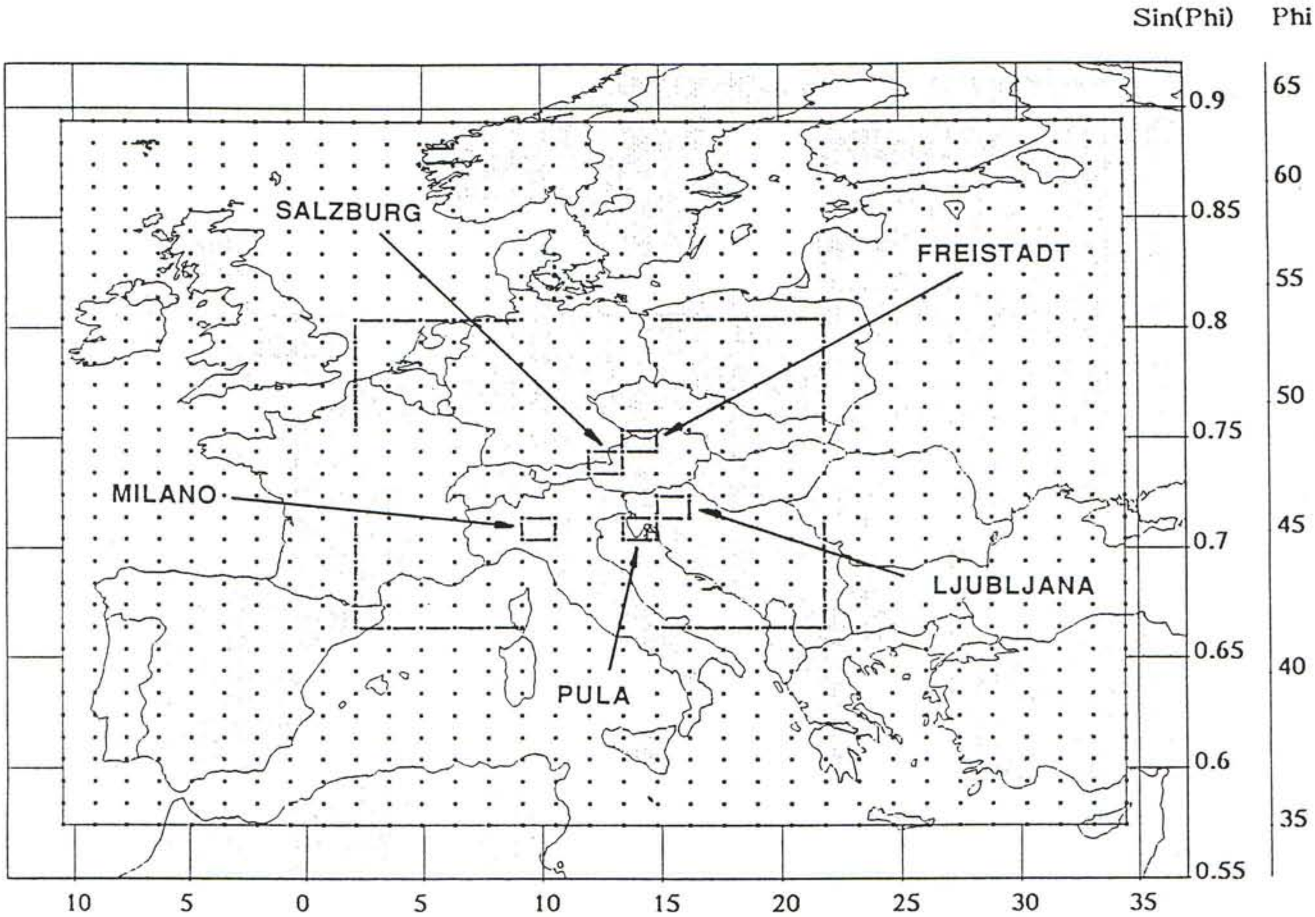

Fig. 2.3. Area of investigation in λ (= longitude), μ (= sin ϕ, ϕ = latitude)-coordinates; divided into 32 × 32 diagnostic columns; framed area and selected individual columns are discussed later.

Abb. 2.3. Untersuchungsgebiet in λ (= geographische Länge), μ (= sinϕ, ϕ = geographische Breite)-Koordinaten; unterteilt in 32×32 diagnostische Säulen; markierte Flächen und Säulen werden später diskutiert.

$$\overset{\infty}{b}_q + \frac{g}{p_s}\,(LH + PREC) + \overset{\infty}{imb}_q = 0 \qquad (2.4)$$

leads to the vertical mean $\overset{\infty}{imb}_q$ of imb_q specified in terms of the vertical mean $\overset{\infty}{b}_q$ of b_q and the surface fluxes $r(p_s) \equiv$ PREC and $f(p_s) \equiv$ LH. Similarly, the vertically averaged thermodynamic equation

$$\overset{\infty}{b}_T + \frac{g}{p_s}\,(SH - PREC) - g\kappa\,(\overset{\infty}{\frac{w(p)}{p}}) + \overset{\infty}{imb}_T = 0 \qquad (2.5)$$

relates the vertical mean $\overset{\infty}{imb}_T$ of imb_T to $\overset{\infty}{b}_T$ and the surface fluxes $w(p_s) \equiv$ SH and PREC. However, due to the subgridscale energy conversion term appearing in eq. (2.2) the vertical mean $\overset{\infty}{imb}_T$ cannot be explicitly determined from eq. (2.5).

Nevertheless, eqs (2.4) and (2.5) allow to obtain the vertical mean imbalances as residuals of the measured gridscale budgets plus surface fluxes; these mean imbalances represent the objectively diagnosed accuracy of the model equations within one column. Therefore, both $\overset{\infty}{imb}_q$ and $\overset{\infty}{imb}_T$ are considered to be measurable. However, the vertical profiles of the imbalances cannot be measured and must be specified.

The vertical profiles of the imbalance terms are specified through the *structure functions* i_q and i_T by the following relationship:

$$imb_{q,T}(p) = i_{q,T}(p)\,\overset{\infty}{imb}_{q,T}. \qquad (2.6)$$

The problem how the structure functions should be specified has been discussed by EMEIS (1985a), HANTEL (1986b) and BURKHARDT (1990). The gross result of these studies has been that imb_q should quasi-exponentially decay from high surface values to zero stratosphere values while for imb_T a vertically constant profile is more appropriate. The vertical profiles of i_q and i_T used in this study are shown in Fig. 2.4.

The next — and major — assumption in the solution process performed in DIAMOD introduces the following coupling between moisture and heat flux:

$$f(p) = \frac{1}{\beta(p)}\,w(p). \qquad (2.7)$$

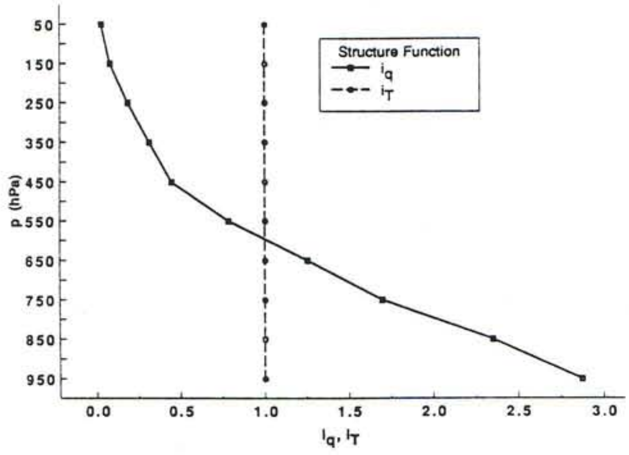

Fig. 2.4. Vertical profiles of structure functions i_q and i_T; profiles constant in each diagnostic column; structure functions are normalized so that their numerical vertical average is unity.

Abb. 2.4. Vertikalprofile von i_q und i_T; Profile konstant in jeder diagnostischen Säule; vertikaler Mittelwert auf 1 skaliert.

This closure assumption may be justified by, and seen in light of, the familiar concept of the Bowen ratio (e.g., BOWEN 1926, STULL 1988) as the quotient of sensible to latent heat flux. The vertical profile of $1/\beta(p)$ chosen in this study is shown in Fig. 2.5. The specification (2.7) is rather restrictive and its influence on the diagnostic results is the objective of further studies (see also Part II). However, it leads to the elimination of the sub-gridscale moisture flux f(p).

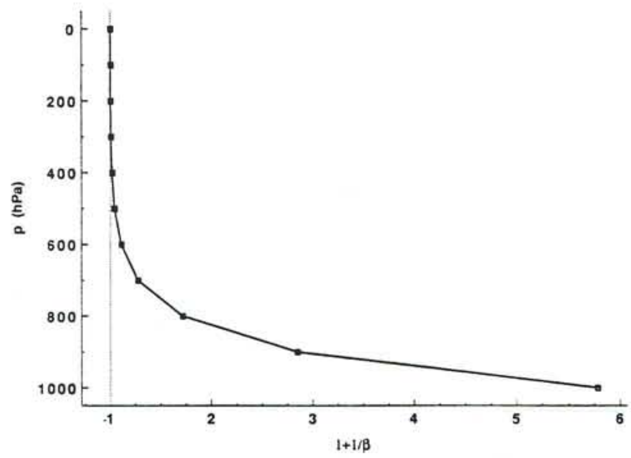

Fig. 2.5. Vertical profile of inverse Bowen-ratio $1/\beta$; surface value given by parameterization of surface sensible and latent heat fluxes; profile constant in each diagnostic column (note: plotted is $1 + 1/\beta$).

Abb. 2.5. Vertikalprofil des inversen Bowen-Verhältnisses $1/\beta$; Bodenwert durch Parametrisierung von LH und SH gegeben; Profile konstant in jeder diagnostischen Säule (beachte: dargestellt ist $1 + 1/\beta$).

Finally, eqs (2.1) and (2.2) are added with the consequence of eliminating r(p). The remaining integral-differential equation:

$$b_q(p) + b_T(p) + g\frac{\partial}{\partial p}\left[\left(\frac{1}{\beta(p)}+1\right)w(p)\right] - g\frac{\kappa}{p}w(p)$$
$$-\, i_q(p)\left[\overset{\infty}{b}_q + \frac{g}{p_s}(LH + PREC)\right]$$
$$-\, i_T(p)\left[\overset{\infty}{b}_T + \frac{g}{p_s}(SH - PREC) - g\kappa\left(\frac{\overset{\infty}{w(p)}}{p}\right)\right] = 0 \qquad (2.8)$$

is solved for the sub-gridscale heat flux w(p) that at this stage represents the only unknown. Once w(p) is known, f(p) is obtained through (2.7), and the vertical rain flux r(p) is obtained by a vertical integration of eq. (2.1) from $p = 0$ to pressure level p with the assumption that the value of the surface rain flux $r(p_s)$ (measured precipitation) is known. At the end of this process the signals s_q and s_T (see Fig. 2.1) are available.

In summary, our approach of obtaining r, f and w from the gridscale moisture and temperature budgets b_q and b_T requires observations of the surface values of these fluxes, namely PREC, LH and SH, respectively (see also Section 3), as well as prescribed vertical profiles of the structure functions $i_q(p)$ and $i_T(p)$ and the inverse Bowen ratio $1/\beta(p)$. The computational process outlined above is also summarized in Fig. 2.1. For its more detailed description — also in connection with the discretized equations — reference is again made to DORNINGER (1992).

3. Meteorological conditions and input data for DIAMOD

As described in the previous section a number of observed quantities are necessary as input to DIAMOD to diagnose sub-gridscale processes. Details of the data used and their preparation are given in this section. This shall be done in terms of actual fields of the first August 1991 days.

3.1 *Meteorological conditions of the August 1991 rain episode*

The synoptic situation of the rain episode in the first August 1991 days is characterized by a dull pressure field without significant gradients, specifically without fronts. Fig. 3.1 shows the surface pressure as analysed by ECMWF. A very weak pressure minimum is located above Central Europe which is almost stationary during this and the following days. The situation is characterized by a moist unstable Mediterranean air mass which is slowly drifting from the southwest into Yugoslavia and further, via Hungary, into Central Europe (STEINACKER, personal communication). The eventual consequence is an orographic lifting of this air north of the Alps. South of the Alps, a relatively dry zone is located over northern Italy with practically no rain.

The 500 hPa field (ECMWF-analysed), reproduced in Fig. 3.2, supports this interpretation. For example, the 560 gpdm-isoline follows the path of the moist unstable air mass. Embedded into the weak trough aloft (Fig. 3.2) are 3

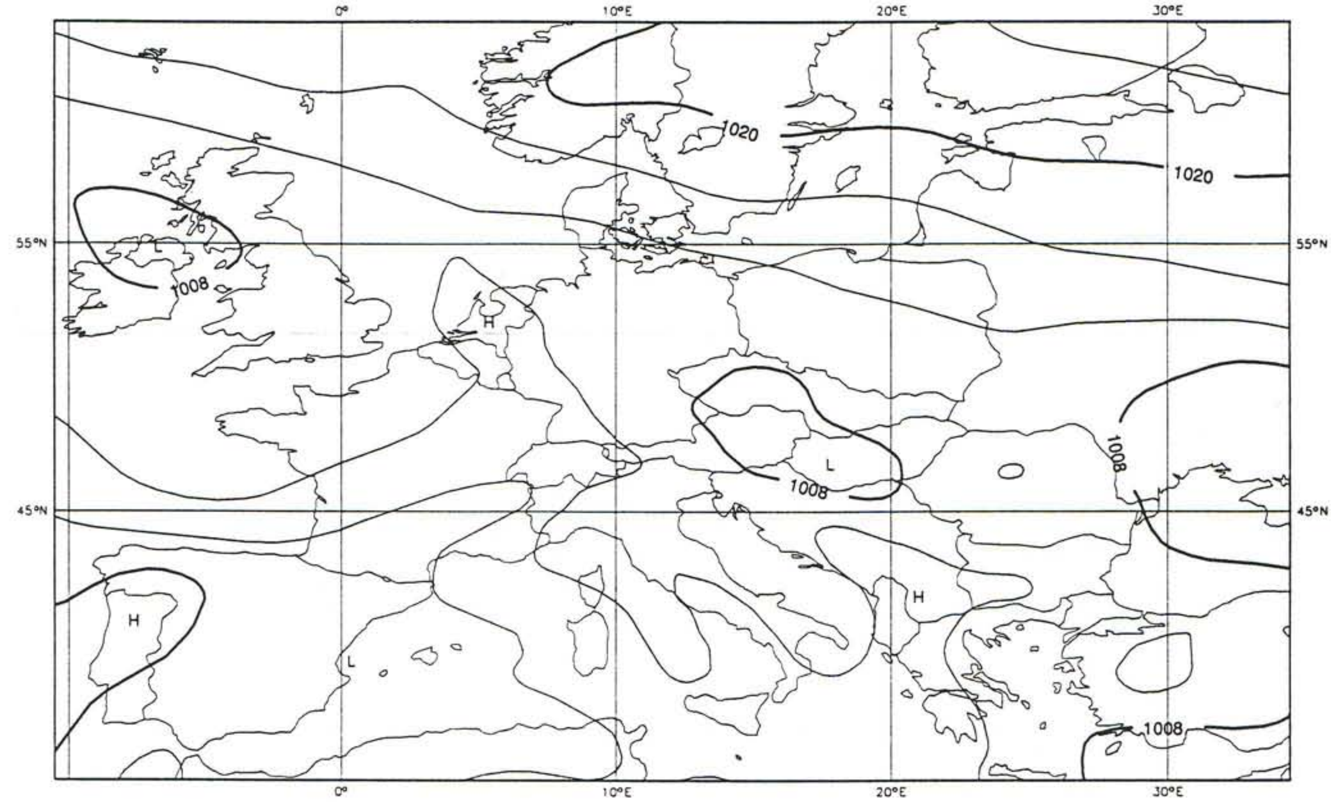

Fig. 3.1. Mean sea level pressure field for 1 August 1991, 00GMT, in units hPa; analysed by ECMWF; contour interval 4 hPa.

Abb. 3.1. Bodendruckfeld vom 1. August 1991, 00GMT, in hPa; analysiert vom EZMW; Konturintervall 4 hPa.

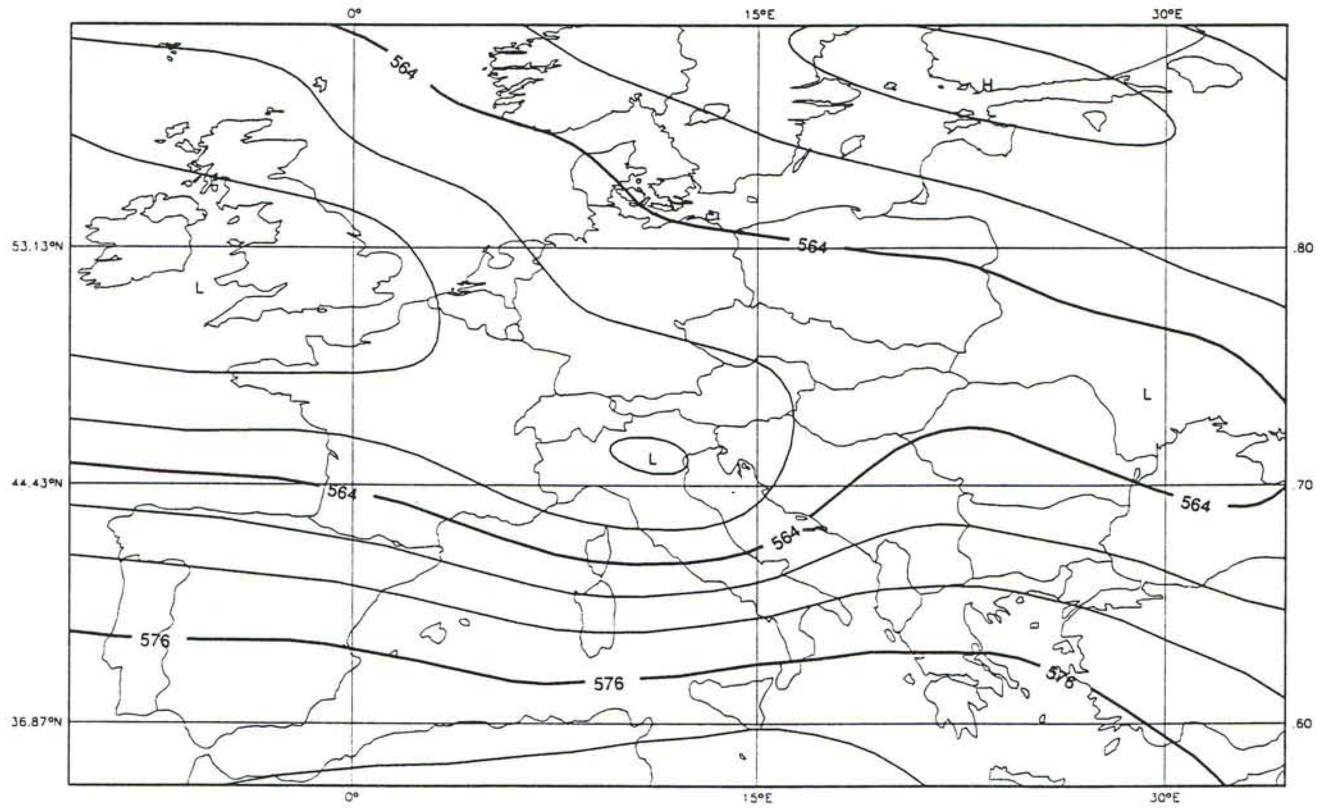

Fig. 3.2. 500 hPa-geopotential field for 1 August 1991, 00GMT, in units 100 m^2/s^2; analysed by ECMWF; contour interval 4 units.

Abb. 3.2. Geopotentialfeld in 500 hPa vom 1. August 1991, 00GMT, in 100 m^2/s^2; analysiert vom EZMW; Konturintervall 4 Einheiten.

regional surface low centers (Fig. 3.1). We may note the correlation between these and the analysed precipitation maxima (Fig. 1.1) over the British Isles, over Austria/Bavaria/Bohemia, and over Western Russia. The two other rain maxima of Fig. 1.1 appear less reliable. It is particularly the precipitation maximum over the North Sea that should be considered with some caution because no surface observation supports its existence. — The observed precipitation field has already been briefly considered from the local viewpoint of Salzburg in the Introduction. It will be discussed in the broader context of objectively analysing the rain observations in Section 3.3.

The arguments above suggest that the meteorological situation during the first August 1991 days can be characterized as tropical. This viewpoint is supported by the equivalent potential temperature field (see Section 7).

3.2 *Gridscale variables*

In order to obtain the gridscale moisture and temperature budgets b_q and b_T as described in Section 2.1 the variables q, T, V and ω must be available on the elementary grid. In addition, the divergence of the net radiative flux R is required.

For the period investigated the fields of q, T, V and ω are derived from the respective non-initialized analysed fields archived at the ECMWF with the exception of the vertical velocity field at the surface [$\omega(p_s)$]. Examples of analysed ECMWF-fields have been reproduced in Figs. 3.1, 3.2.

The vertical velocity at the surface requires special attention because the archived field at ECMWF is obtained by vertical integration of the continuity equation which may lead to erroneous results. Therefore, the field of $\omega(p_s)$ is taken in this study as the time tendency (over twelve hours) of the pressure at the ground derived from the mean-sea-level pressure analysis at the ECMWF. This $\omega(p_s)$ is then attributed to the $p_s = 1000$ hPa-level which introduces a slight inconsistency into our input data.

Our approach here is equivalent to neglecting the surface topography at the lower boundary of the DIAMOD atmosphere. The impact of this approximation upon the results, specifically upon the vertical sub-gridscale fluxes, is proportional to the relative overestimation of the mass in the column; however, the net effect is surprisingly small. For example, SHAO & HANTEL (1986) have demonstrated for the momentum budget that the vertical flux diagnosed as residual from the budget is just marginally influenced by incorporating the mass reduction necessary for the lowest layer over areas with pronounced orography like, for example, the Alps. Their horizontal patterns of the vertical sub-gridscale momentum flux in the free atmosphere could not be visibly distinguished from each other if the mass reduction due to orography was switched on or off.

From the spectrally archived fields at given pressure levels values on the grid point locations of the elementary grid are obtained by the usual transformation from spectral space into physical space. Then, a linear interpolation is used in the vertical to obtain values of the variables at the 50 hPa spacing of the elementary grid.

This interpolation process is introducing errors in the windfield such that the continuity equation (2.3) is no longer exactly satisfied. Therefore, at the point when mass fluxes are computed on the diagnostic grid, it is necessary to remove the resulting noise divergences (see also Section 2.2). In general, due to the high quality of the analysed data used, the modification required is rather small. Typically, in an rms-sense the necessary modifying mass flux is about 5 % (see also WANG et al. 1992).

This mass flux modification module of DIAMOD is the main instrument to guarantee that the impact of identifying the lower boundary with the 1000 hPa-surface instead of the observed p_s is of little concern for the budgets; this applies to all layers except the lowest. The budget and the sub-gridscale fluxes are governed by the divergent part of the mass flux field. As long as the mass flux field is strictly nondivergent in the 3D-sense the budget is relatively insensitive to the remaining mass flux errors.

Referring back to Figs. 3.1 and 3.2 it is noted that these figures show pressure and geopotential fields for the temporal mid-point (i.e., 1. August 1991, 00GMT) of the 12h time interval for which the surface precipitation is shown in Fig. 1.1 which is appropriate regarding the individual nature of these fields.

Concerning the net radiative flux R, its divergence is taken in this study to be vertically constant with a value of 10 W/m^2 per 100 hPa. For the time intervals of about 12 hours under consideration this crude approximation seems to be adequate, also in view of similar values obtained by prognostic models (e.g., ECMWF). However, an investigation of a more sophisticated radiative scheme might prove useful.

3.3 *Surface precipitation*

The values of the rain flux at the surface $r(p_s)$ = PREC representative for the horizontal area of a diagnostic box are derived by an iterative algorithm (CRESSMAN 1959) from operational precipitation measurements reported every twelve hours. The number of observations available for this estimation of PREC is about 1000 with the spatial distribution shown in Fig. 3.3. This coverage implies, on the average, about 1 station per diagnostic column. However, the data coverage is rather high in Central Europe so that PREC can be estimated quite well there.

The surface precipitation accumulated during 12 hours over the full domain under investigation is shown in Fig. 3.4 for the period starting at 31 July 1991 and ending at 3 August 1991. It is evident from these pictures that rain rates exceeding 40 mm/12h occurred on 1 and 2 August 1991 in the vicinity of Salzburg; these analyses are done on the elementary grid and values are therefore representative for an area of about (50 km)^2. Further, Figs. 3.4c and 1.1 allow to compare the differences in analysed surface precipitation if the analysis algorithm is run on the elementary grid (Fig.

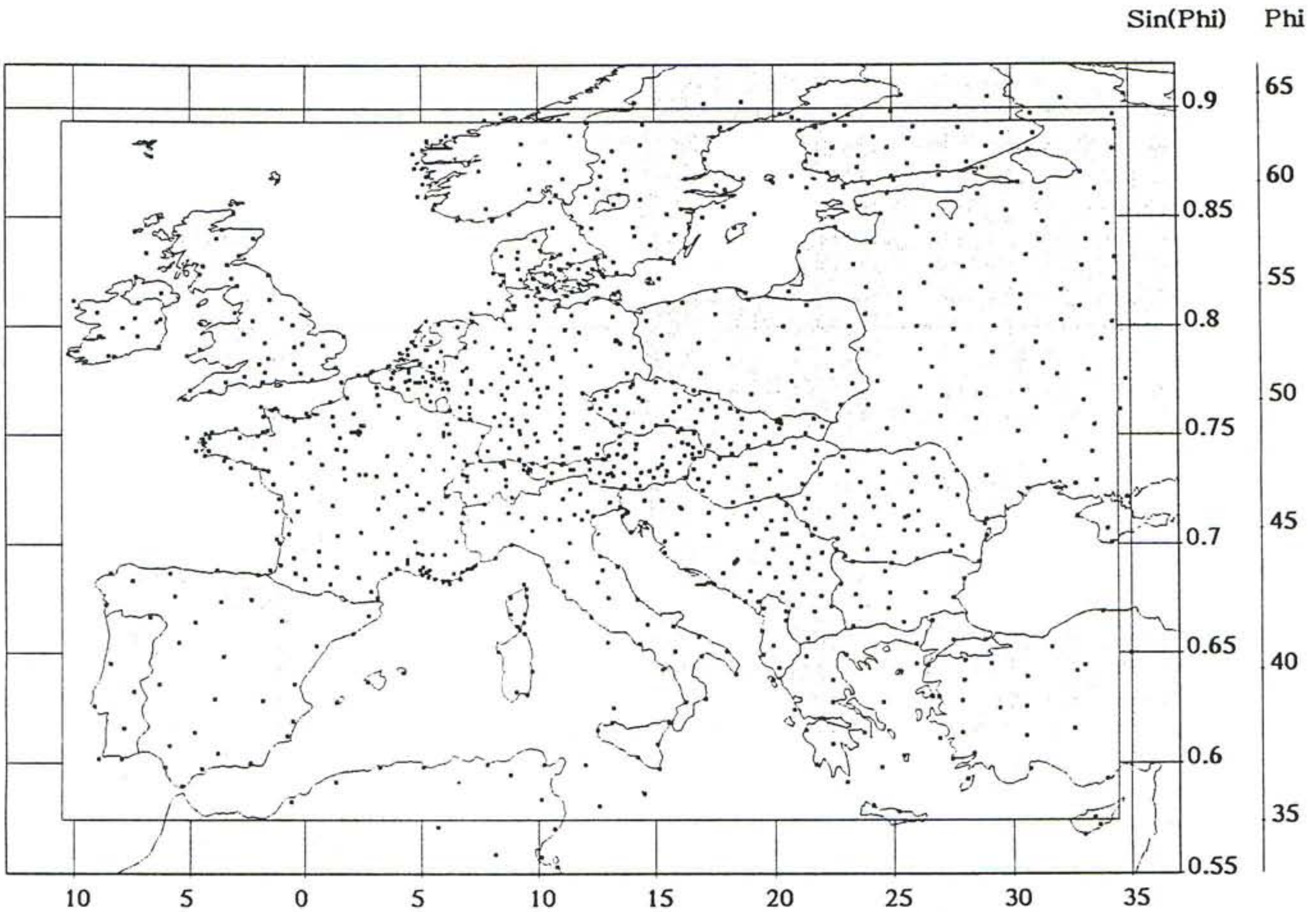

Fig. 3.3. SYNOP-network over Europe; reports of these stations are used for analysing the surface precipitation.

Abb. 3.3. SYNOP-Meßnetz über Europa, Meldungen dieser Stationen werden zur Analyse des Bodenniederschlages verwendet.

3.4c) and on the diagnostic grid (Fig. 1.1). It is evident that the latter is characterized by a smoother structure.

The surface rain PREC for the twelve-hour periods (derived from the rain rates) centered at 1 and 2 August 1991, 00 GMT, is shown in Fig. 3.5. These quantities — representative for areas of (100 km)^2 — enter DIAMOD in the way described in Section 2.2. Whereas the surface rain flux attains values of almost 2000 W/m^2 during the night from 31 July to 1 August 1991 in the vicinity of Salzburg, it decreases to about 1000 W/m^2 during the following night. The remarkable magnitude of these surface fluxes is one of the main reasons for the attention paid to this particular case.

3.4 *Latent and sensible heat flux*

Compared to the effort to specify the measured surface rain flux, the scheme to obtain LH and SH is rather simple. In particular, these values are taken as constant in time and space and are assigned values of —82 W/m^2 and —17 W/m^2, respectively. Thus, both fluxes are rather small at the surface (close to climatology) and upward. The inverse Bowen ratio is approximately 4.8 (see also Fig. 2.5). The smallness and constancy of both fluxes must be seen in light of the large values of PREC. In particular, it is argumented that evaporation must be small in the presence of heavy rain. However, a more realistic specification of LH and SH (e.g., HOLTSLAG & VAN ULDEN 1983) will be the subject of further study (see also Section 7.1).

Fig. 3.4. Sequence of surface precipitation fields over Europe from a) 31 July 1991, 06GMT, to h) 3 August 1991, 18GMT, in units mm/12h; precipitation measured at end of time interval (= time indicated); reported through SYNOP-network (compare Fig. 3.3) and objectively analysed on elementary grid with CRESSMANN method; contour interval 5 mm/12h; isoline 1 mm/12h bold.

Abb. 3.4. Zeitreihe von Niederschlagsfeldern über Europa vom a) 31. Juli 1991, 06GMT, bis h) 3. August 1991, 18GMT, in mm/12h; gemessen am Ende des Zeitintervalls (= angegebene Zeit); erhoben durch das SYNOP-Meßnetz (vgl. Abb. 3.3) und objektiv mittels CRESSMAN-Methode auf das Elementargitter analysiert; Konturintervall 5 mm/12h; 1 mm/12h-Isolinie dick.

a) DATE: 91073106 STATISTICS: MEAN= .85; RMS= 3.04; VAR= 2.92 .

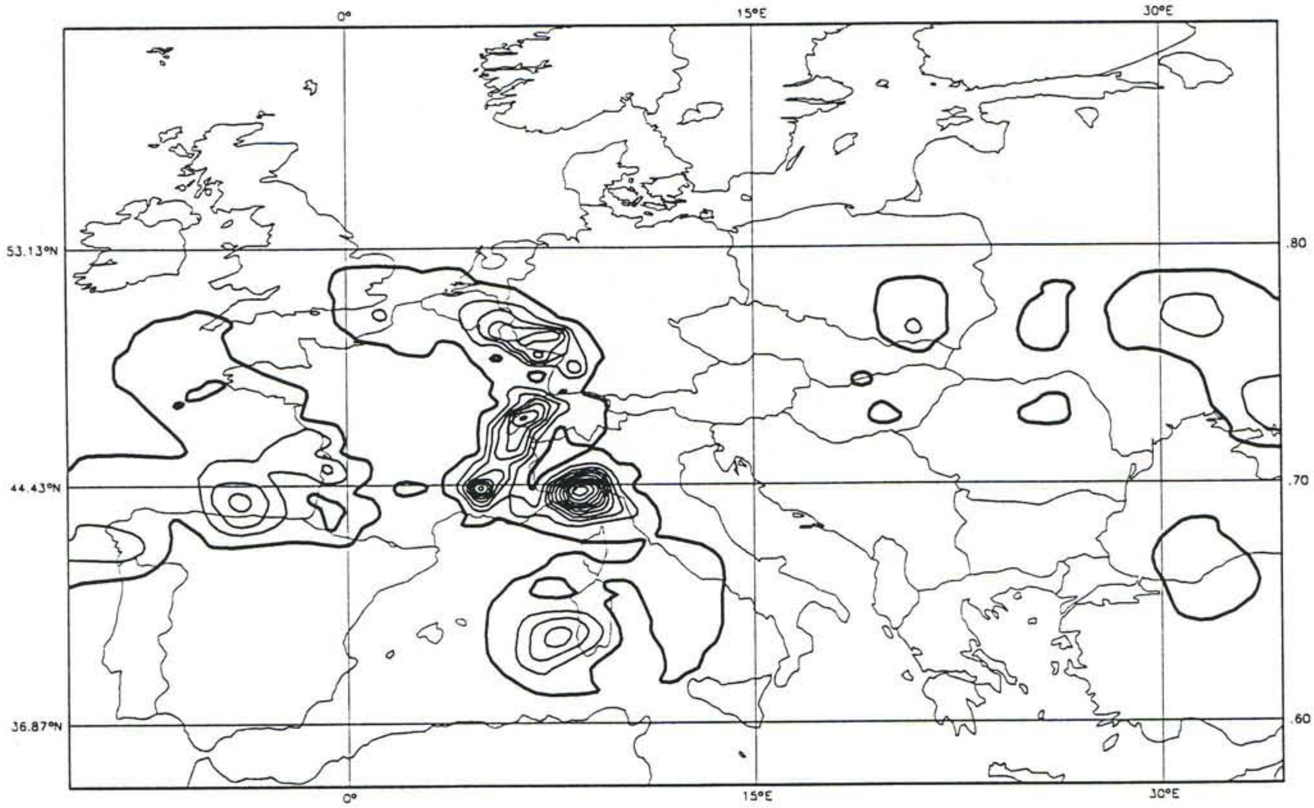

b) DATE: 91073118 STATISTICS: MEAN= .91; RMS= 2.97; VAR= 2.83 .

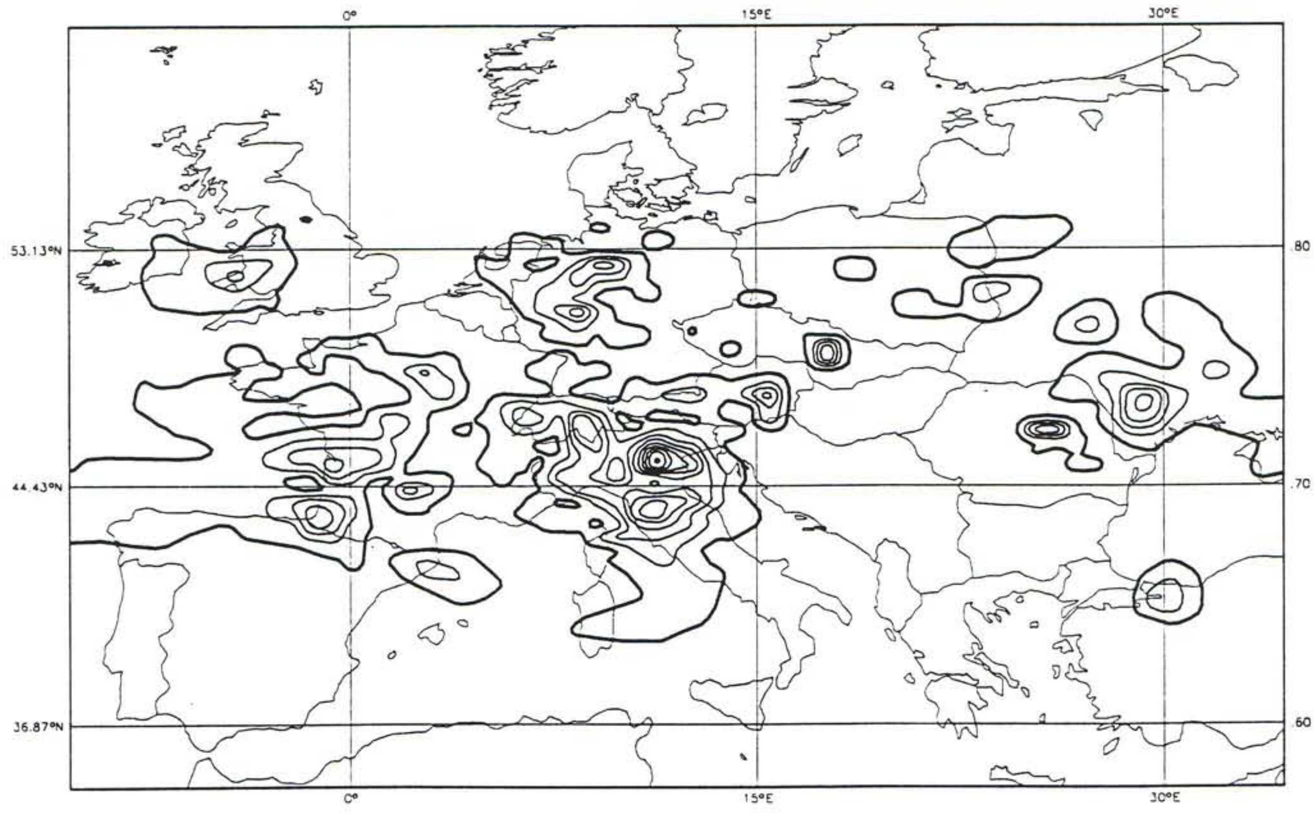

c) DATE: 91080106 STATISTICS: MEAN= 1.50; RMS= 4.83; VAR= 4.59 .

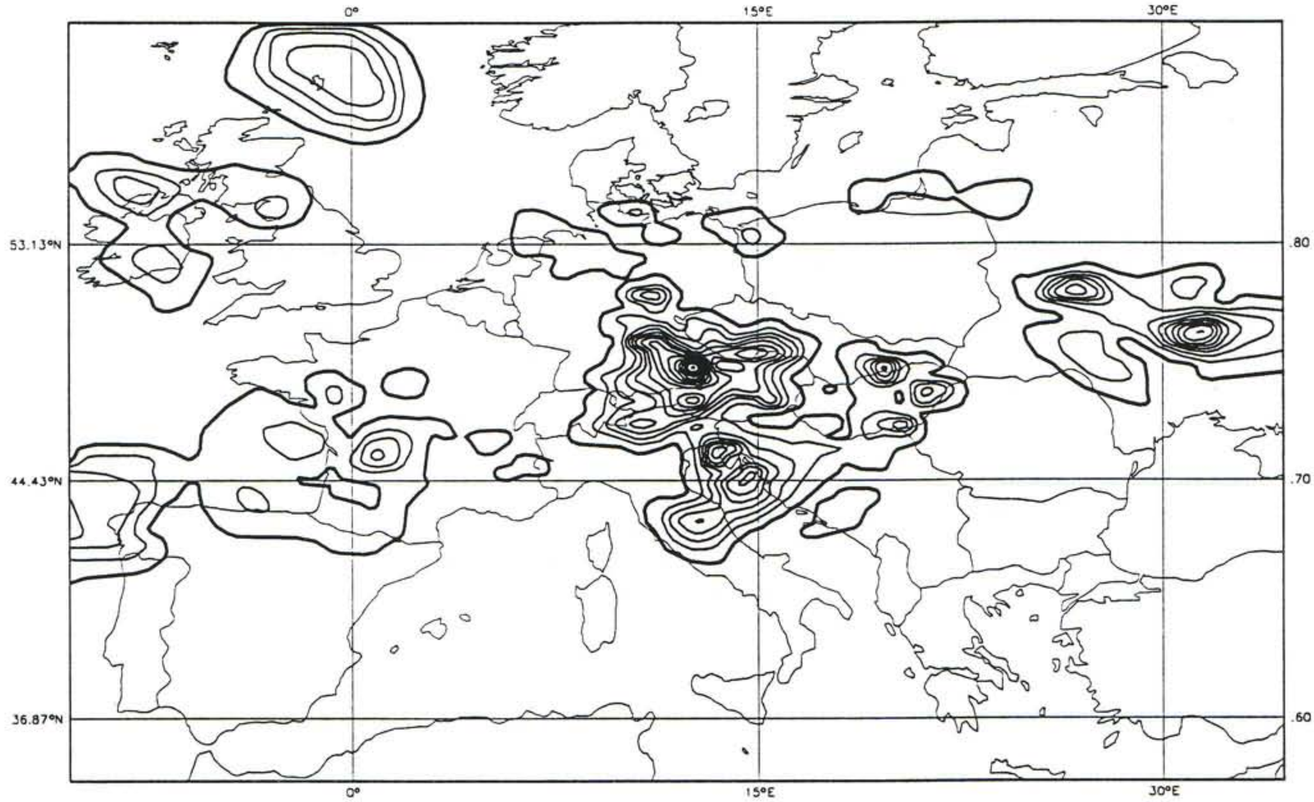

d) DATE: 91080118 STATISTICS: MEAN= 1.08; RMS= 3.54; VAR= 3.37 .

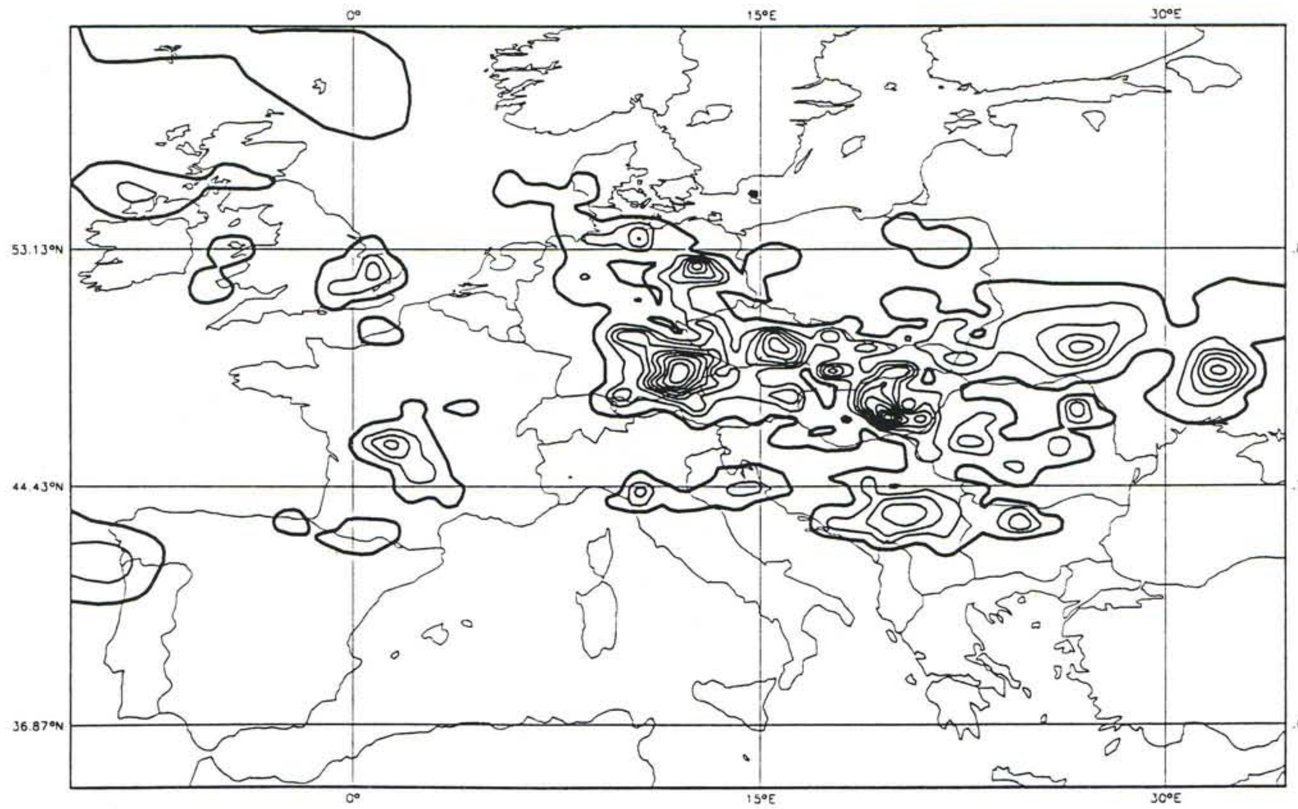

e)　DATE: 91080206　　STATISTICS: MEAN= .78; RMS= 2.98; VAR= 2.88 .

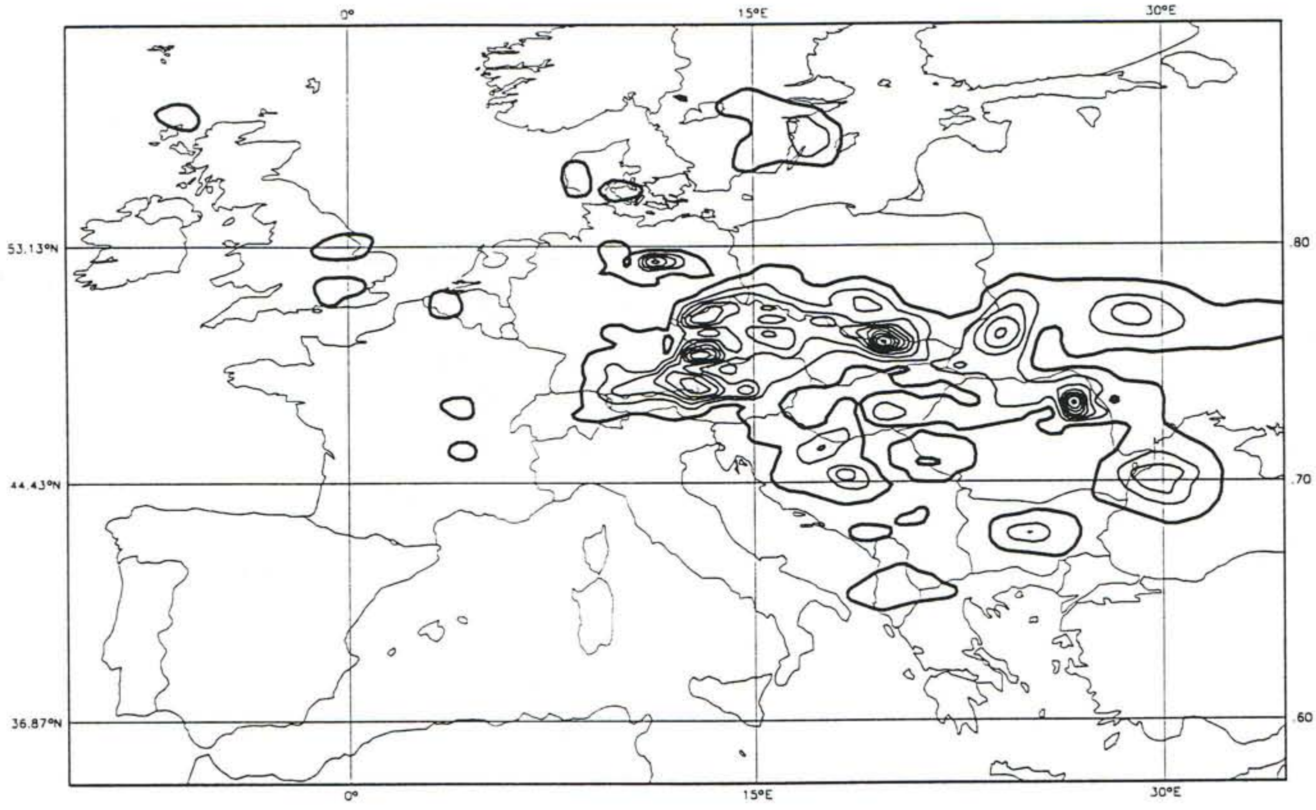

f)　DATE: 91080218　　STATISTICS: MEAN= .89; RMS= 3.22; VAR= 3.10 .

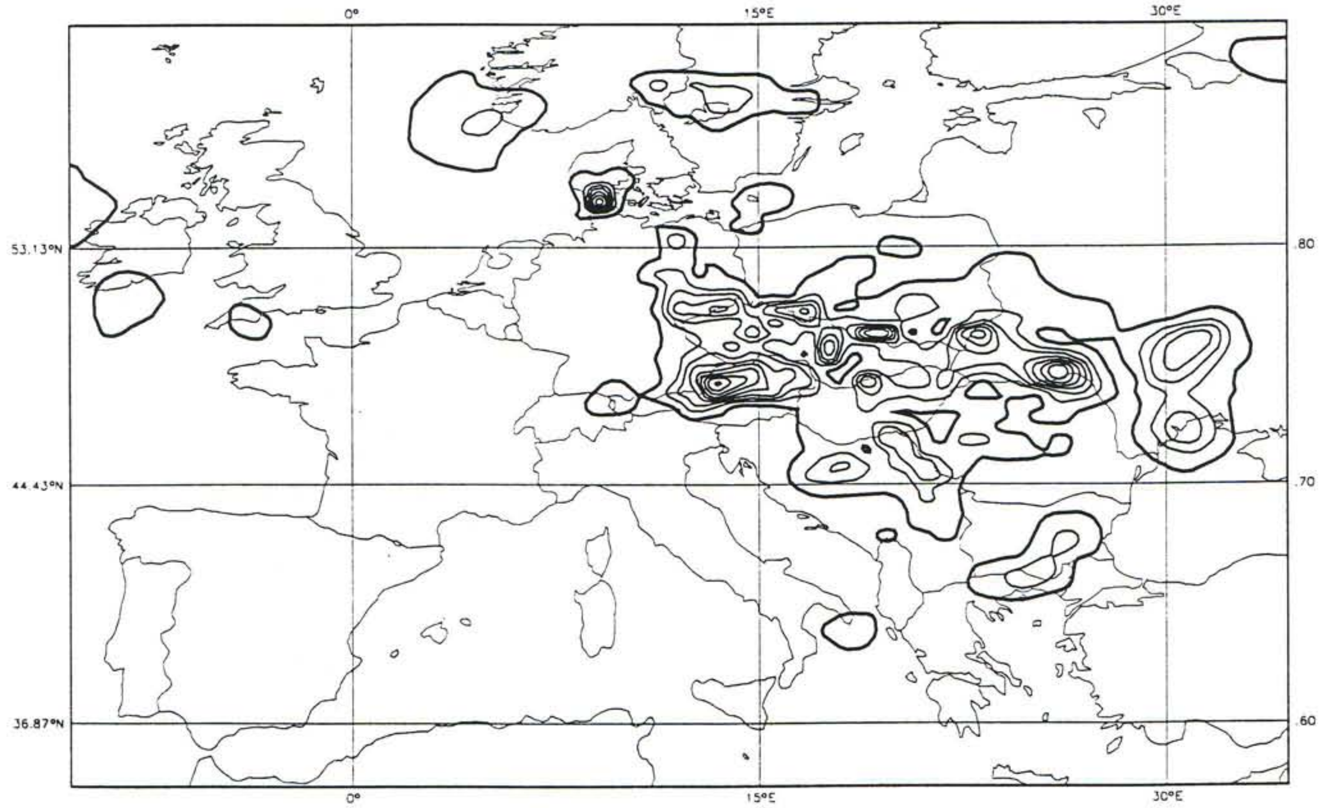

g) DATE: 91080306 STATISTICS: MEAN= .62; RMS= 2.75; VAR= 2.68 .

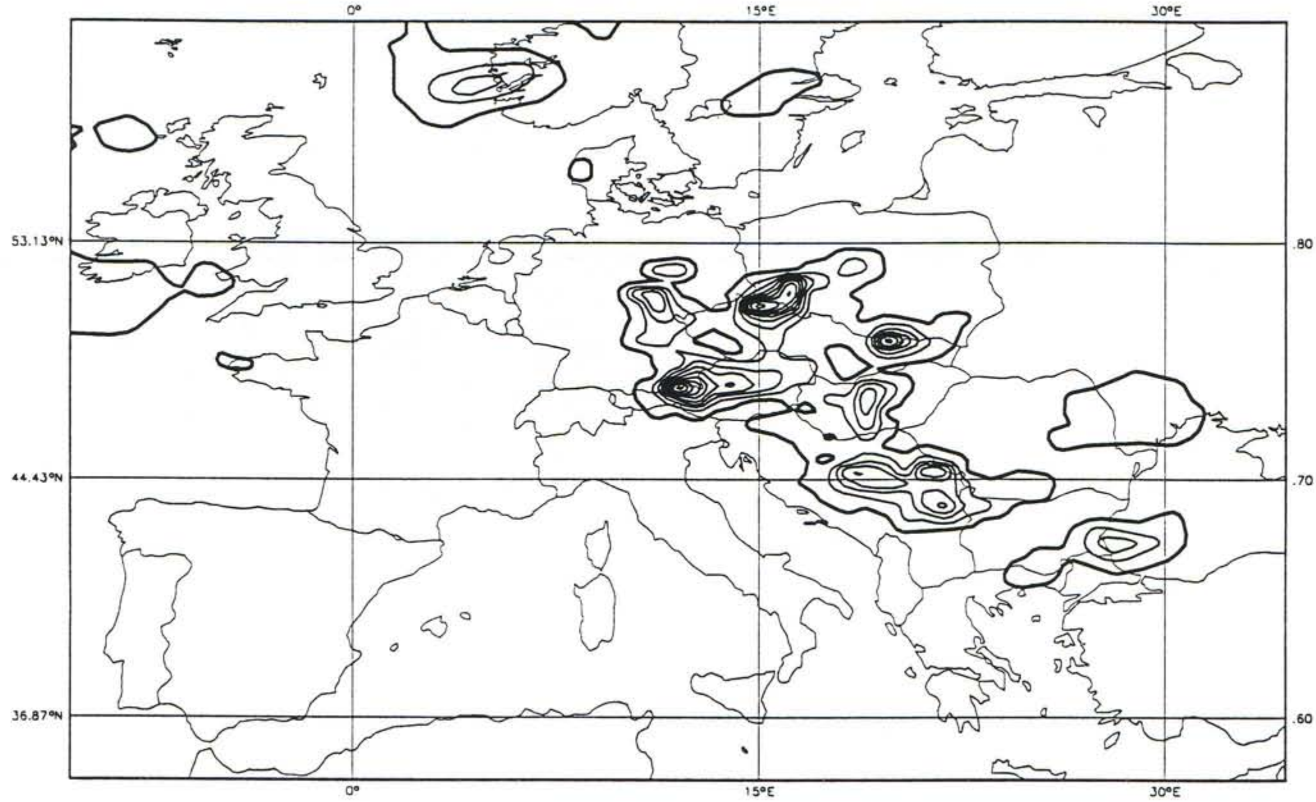

h) DATE: 91080318 STATISTICS: MEAN= .61; RMS= 2.17; VAR= 2.09 .

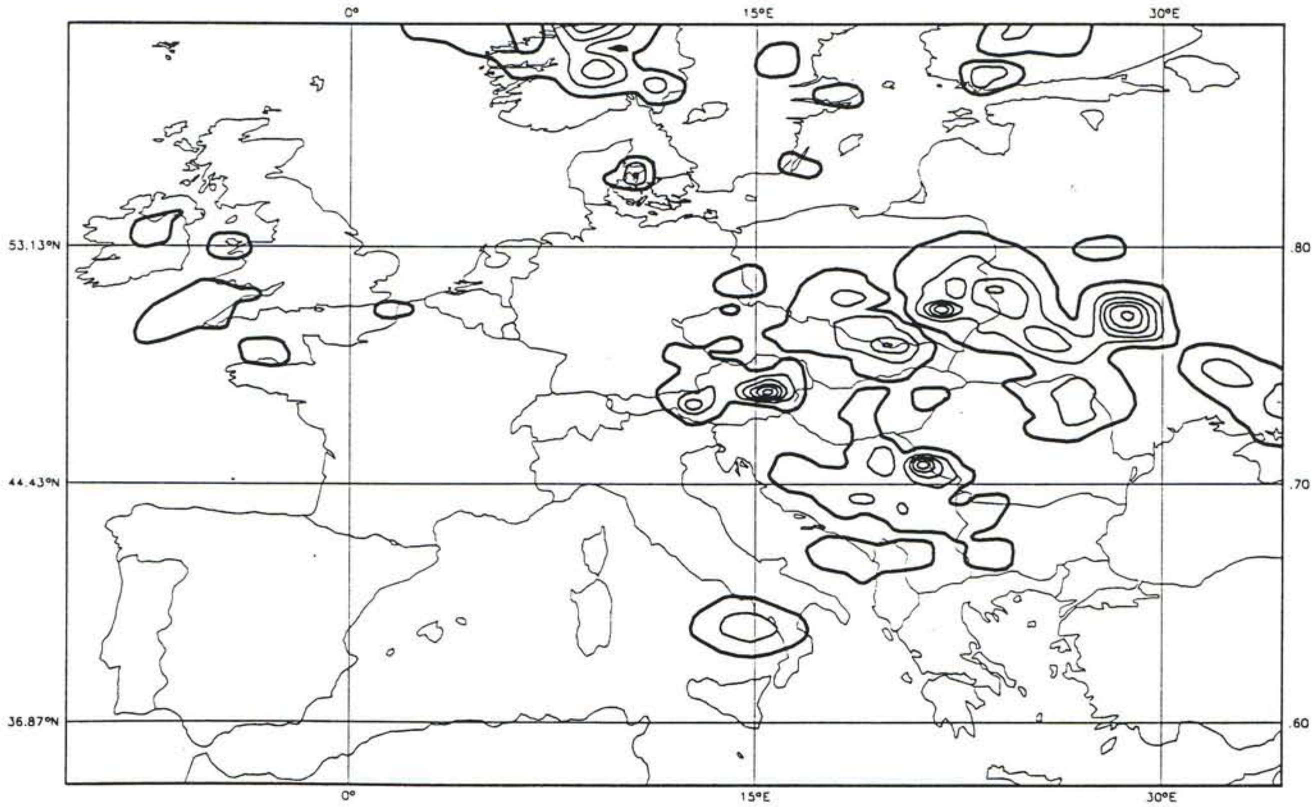

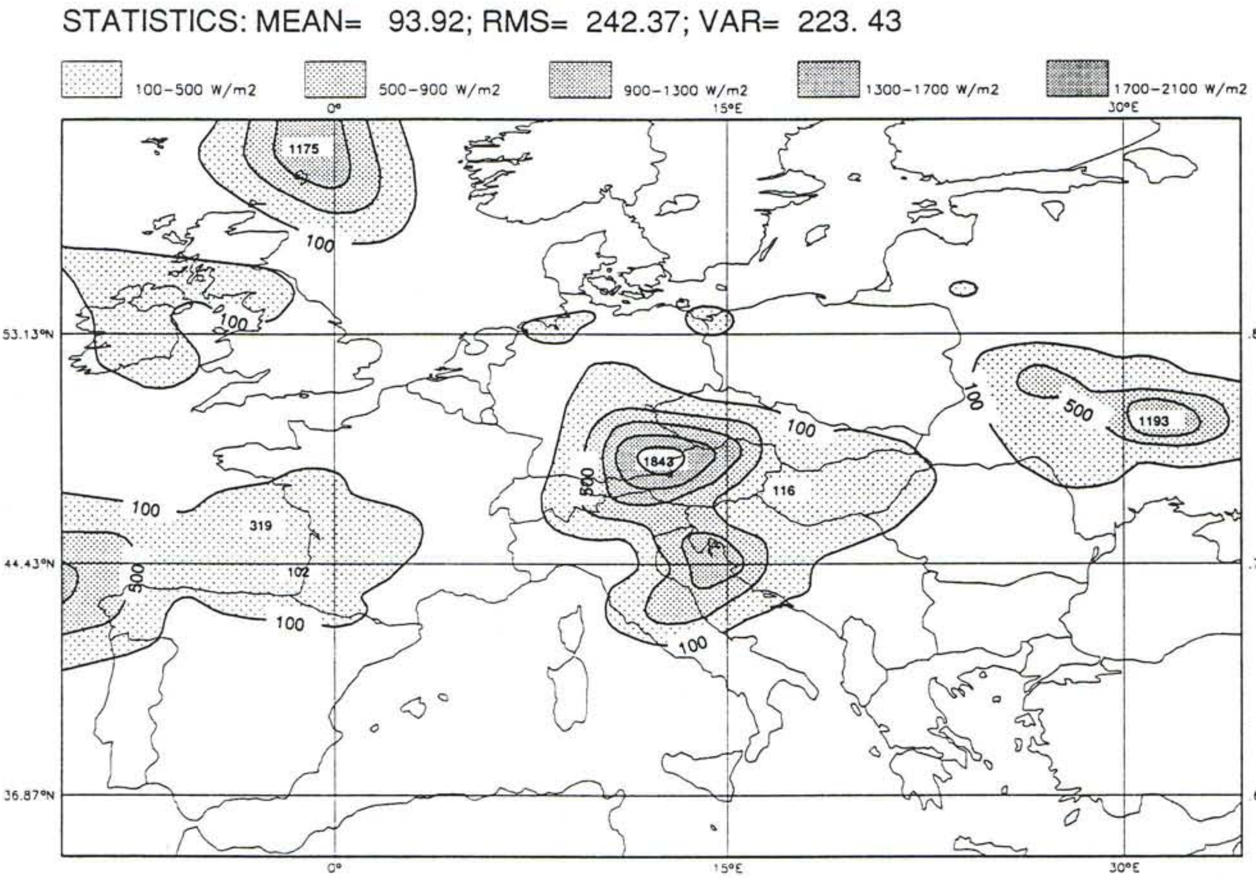

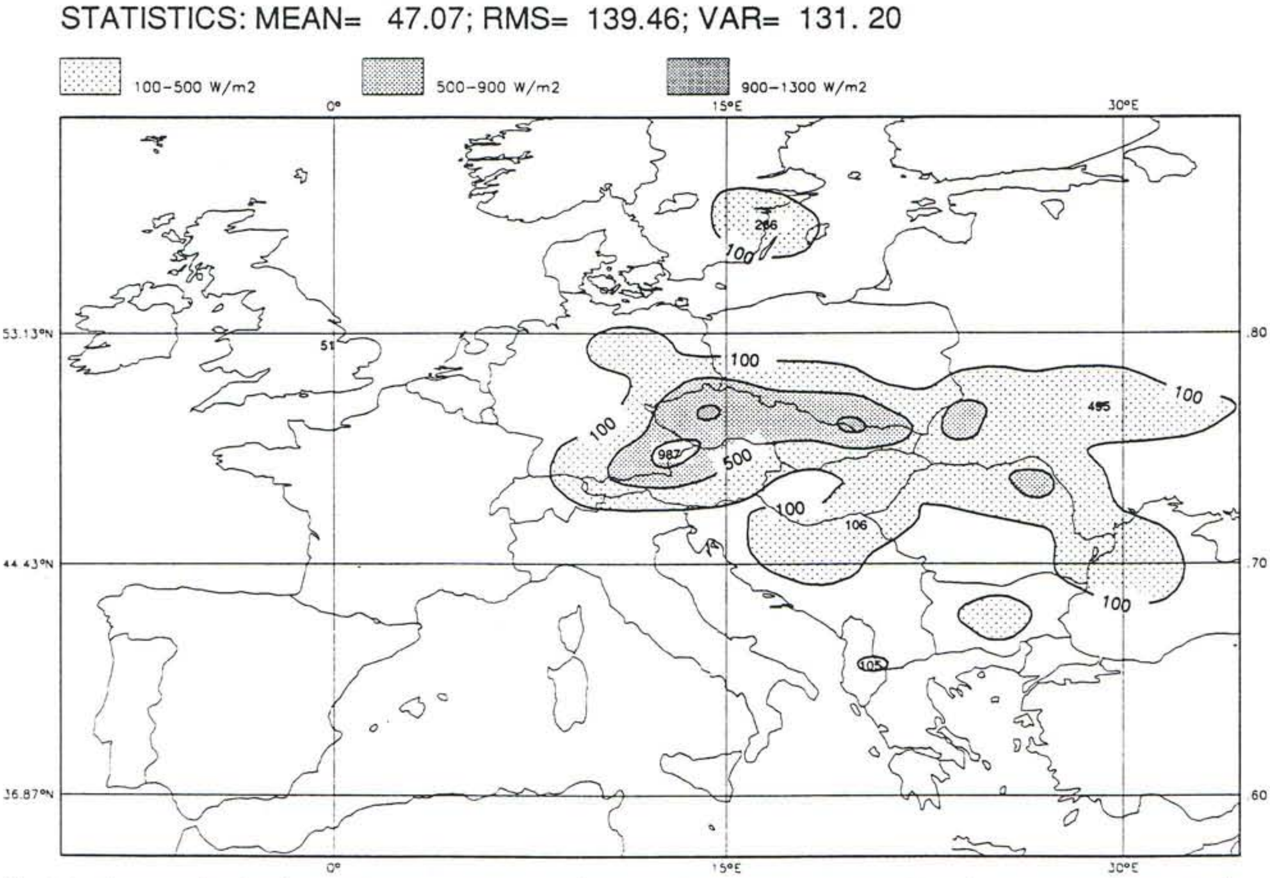

Fig. 3.5. 12h-accumulated surface precipitation over Europe for a) 1 August 1991, 00GMT ± 6h (compare Fig. 1.1), and for b) 2 August 1991, 00GMT ± 6h, in units W/m²; contour interval 400 W/m²; note: 100 W/m² ≈ 1.7 mm/12h.

Abb. 3.5. Bodenniederschlag über Europa aufsummiert über 12h vom a) 1. August 1991, 00GMT ± 6h (vgl. Abb 1.1), und vom b) 2. August 1991, 00GMT ± 6h, in W/m²; Konturintervall 400 W/m²; beachte: 100 W/m² ≈ 1.7 mm/12h.

4. Typical diagnostic results for the SALZBURG column

We shall begin to discuss the results of this study with considering the column SALZBURG (for location see Fig. 2.3) for 1 August 1991. As mentioned in the Introduction, the country of Salzburg received the maximum precipitation of this rain period.

Fig. 4.1 shows the main output of DIAMOD: vertical profiles of the sub-gridscale fluxes of rain, moisture and heat for the 12 hour period 31 July, 18GMT until 1 August, 06GMT. Surface rain is PREC = 1670 W/m². The rain flux r has no appreciable values from the uppermost atmospheric levels down to about 300 hPa. Further downward r increases rapidly to its peak at the earth's surface.

While r is downward directed throughout the atmosphere, both f and w are upward. Their surface values are LH = −82 W/m², SH = −17 W/m²; they are kept constant throughout this study (in contrast to the surface value of r which is different from column to column, see also Section 3.3). Further up in the atmosphere, f is maximum across 800 hPa with a value of −409 W/m² while w peaks in 600 hPa with −1132 W/m². There is still an upward w of more than −600 W/m² across 200 hPa.

The results of this column are relatively accurate. The rms-value of imb_q is 14 W/m², of imb_T it is 20 W/m².

Both f and w are much larger in the free atmosphere than across the earth's surface. This demonstrates that the vertical sub-gridscale fluxes are determined by, and are indispensible parts of, the atmospheric box budgets; the sub-gridscale fluxes are certainly not controlled by their respective surface values. This justifies our present procedure to specify LH and SH from climatological estimates which severely limits their accuracy.

The profile of the rain flux r, on the other hand, depends critically upon the measured surface value PREC. First, PREC controls the scale of r(p). Second, the error of PREC controls mainly the size of both imbalances imb_q and imb_T. Thus, the combination of a sizeable r(p) with a relatively small imbalance is a good criterion for the credibility of a result as presented in Fig. 4.1.

We proceed by investigating the other heat budget terms which are the background for the profiles of Fig. 4.1. Fig. 4.2 shows the three components of the moisture budget for the SALZBURG column, again for the 12 hour period 31 July, 18GMT until 1 August, 06GMT. While the fluxes of Fig 4.1 are valid across the pressure level indicated, the budget quantities of Fig. 4.2 represent vertical integrals over 100 hPa-layers. Fig. 4.2 exhibits a b_q that is negative throughout the lower troposphere; it represents a gridscale moisture convergence of about −300 W/m² per 100 hPa-layer up to 500 hPa. As mentioned above, the box imbalance is relatively small; according to our error model (see Section 2) it is maximum in the lowest pressure layer (42 W/m²) and decreases exponentially upward. Consequently, the signal s_q is determined by, and opposite to, the budget; it is not contaminated by any sizeable error.

This can be seen more clearly from Fig. 4.3 in which the budget components are further decomposed and given by their numerical values; Fig. 4.4 shows the corresponding

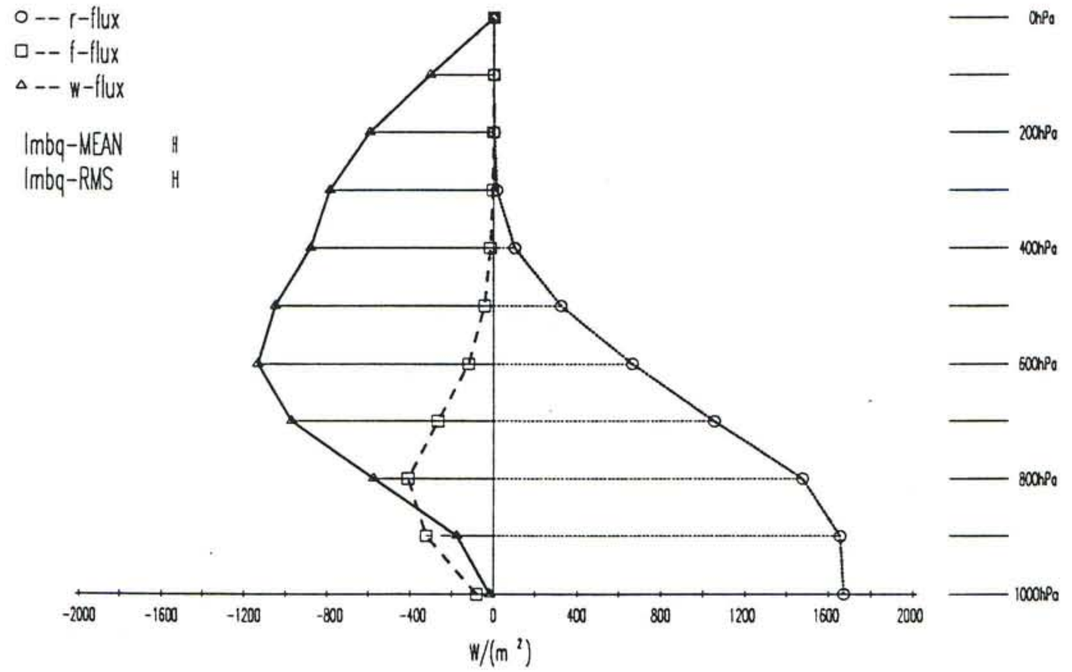

Fig. 4.1. Vertical profiles of r, f and w in column SALZBURG (for position see Fig. 2.3) for 1 August 1991, 00GMT ± 6h, in units W/m²; upward fluxes negative, downward fluxes positive; symbols indicate diagnosed fluxes through given level.

Abb. 4.1. Vertikalprofile von r, f und w der Säule SALZBURG (zur Lokalisierung s. Abb. 2.3) vom 1. August 1991, 00GMT ± 6h, in W/m²; aufwärtsgerichtete Flüsse negativ; abwärtsgerichtete Flüsse positiv; Symbole geben diagnostizierten Fluß durch angegebenes Niveau an.

fluxes in horizontal and vertical directions across all faces of each diagnostic box of the column SALZBURG. The quantities of b_q and imb_q are displayed in both Figs. 4.2, 4.3, and r(p) and f(p) are displayed in both Figs. 4.1, 4.4. However, for the sake of clarity we shall tolerate this redundancy in this specific example. The first information in Fig. 4.3 that is new relative to Fig. 4.1 is the decomposition of b_q into *moisture tendency* and 3D-*moisture flux divergence* [see also eq. (2.1)]. Both are negative in the entire column. While the negative tendency with its drying effect dominates in the lower layers up to 800 hPa, the negative moisture flux divergence governs the latent heat budget in the middle and upper troposphere. The second additional information in Fig. 4.3 is the decomposition of the signal s_q (see also Fig. 2.1) into the divergences of sub-gridscale moisture and rain flux. For the sake of clarity, note that, for example, $L\partial\overline{q'\omega'}/\partial p$ in the layer 900—1000 hPa actually stands for the vertical integral of this quantity over this layer and thus represents, strictly spoken, not a flux *divergence* but a flux *difference*; in this case, $L\partial\overline{q'\omega'}/\partial p$ represents f(1000 hPa) —f(900 hPa) = —82 W/m² — (—322 W/m²) = 240 W/m². Similarly, in the same layer, $gL\partial\bar{P}/\partial p$ represents the difference r(1000 hPa) — r(900 hPa) = 1670 W/m² — 1654 W/m² ≈ 17 W/m².

For the sake of simplicity we shall, nevertheless, in discussing integrated box budgets like the ones in Figs. 4.2, 4.3, adopt the convention to speak not of flux *differences* but of *divergences*. Likewise, we shall continue to speak of *tendencies* although these are actually volume-integrated. Guided by the discussion above a quantitative conversion of the respective budget component into its proper form is possible.

Returning now to the physical content of Fig. 4.3, we see that the sub-gridscale moisture flux is divergent in the lower layers up to 800 hPa and convergent higher up. Further, the rain flux is divergent throughout the entire column with values exceeding 200 W/m² per 100 hPa in the layer 400—800 hPa. The peak value 420 W/m² shows that the maximum condensation rate is located in the layer 700—800 hPa. This demonstrates that DIAMOD allows to locate the layers in which precipitation is actually generated. While we maintain that the meteorological conditions of this case were tropical in character the condensation maxima in the actual tropics may reach even higher up in cases of deep convection (e.g., BURKHARDT 1991).

Concerning the 3D-moisture fluxes displayed in Fig. 4.4 the horizontal gridscale flux is in general smaller than the vertical gridscale flux. Further, it is the gridscale resolved budget terms that in the first place feed the rain. In vertical direction, the sub-gridscale moisture flux is larger or about equal to the gridscale flux in the lowest layers. These results should demonstrate that all components of the moisture budget are very active in the SALZBURG column reaching to quite high levels which is the basis for the strong surface precipitation.

Concerning the T-budget, which is intimately coupled to the q-budget and, in DIAMOD, is evaluated simultaneously, Fig. 4.5 is the temperature equivalent to Fig. 4.2. Accord-

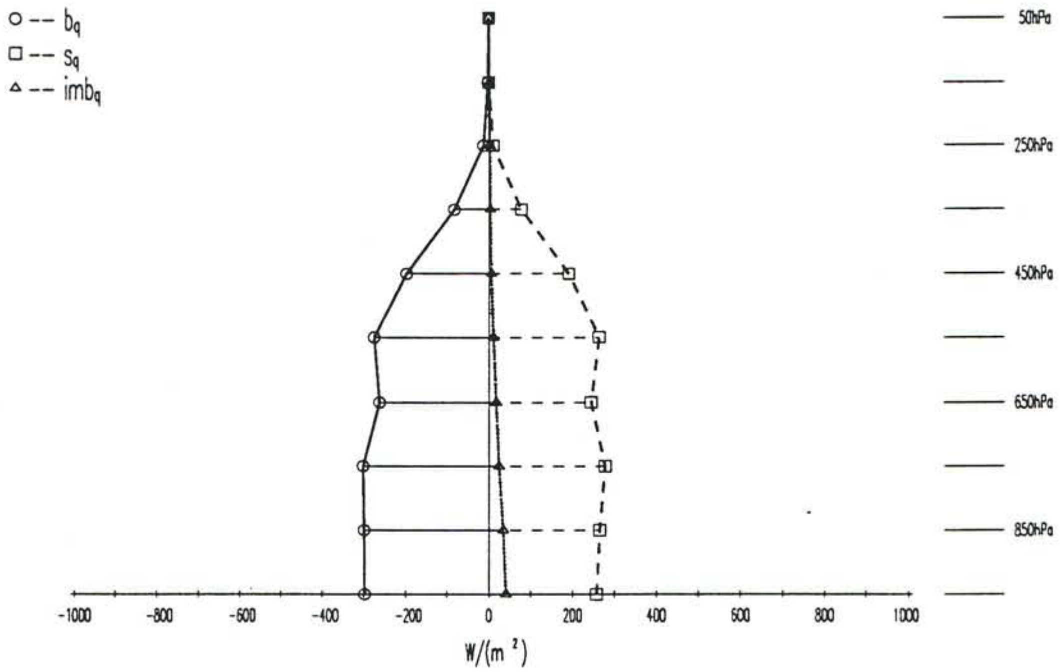

Fig. 4.2. Vertical profiles of b_q, s_q and imb_q in column SALZBURG (for position see Fig. 2.3) for 1 August 1991, 00GMT ± 6h, in units W/m²; values given by symbols are centered in middle of corresponding diagnostic box (e.g., circle plotted in 850 hPa with value b_q = —299 W/m² stands for vertical integral of b_q over pressure layer 800 hPa to 900 hPa).

Abb. 4.2. Vertikalprofile von b_q, s_q und imb_q der Säule SALZBURG (zur Lokalisierung s. Abb. 2.3) vom 1. August 1991, 00GMT ± 6h, in W/m²; durch Symbole gekennzeichnete Werte sind in der Mitte der entsprechenden diagnostischen Box angegeben (z. B., Kreis in 850 hPa mit b_q = —299 W/m² stellt das vertikale Integral von b_q von 800 hPa bis 900 hPa dar).

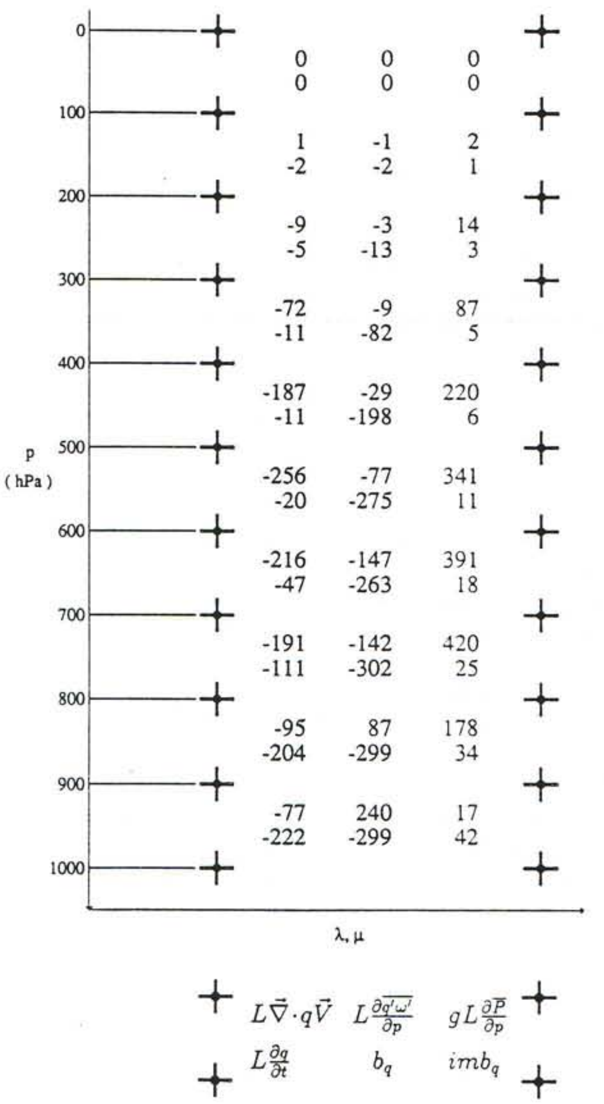

Fig. 4.3. Components of q-budget in each diagnostic box of column SALZBURG (for position see Fig. 2.3) for 1 August 1991, 00GMT ± 6h, in units W/m².

Abb. 4.3. Komponenten des q-Budgets in jeder diagnostischen Box der Säule SALZBURG (zur Lokalisierung s. Abb. 2.3) vom 1. August 1991, 00GMT ± 6h, in W/m².

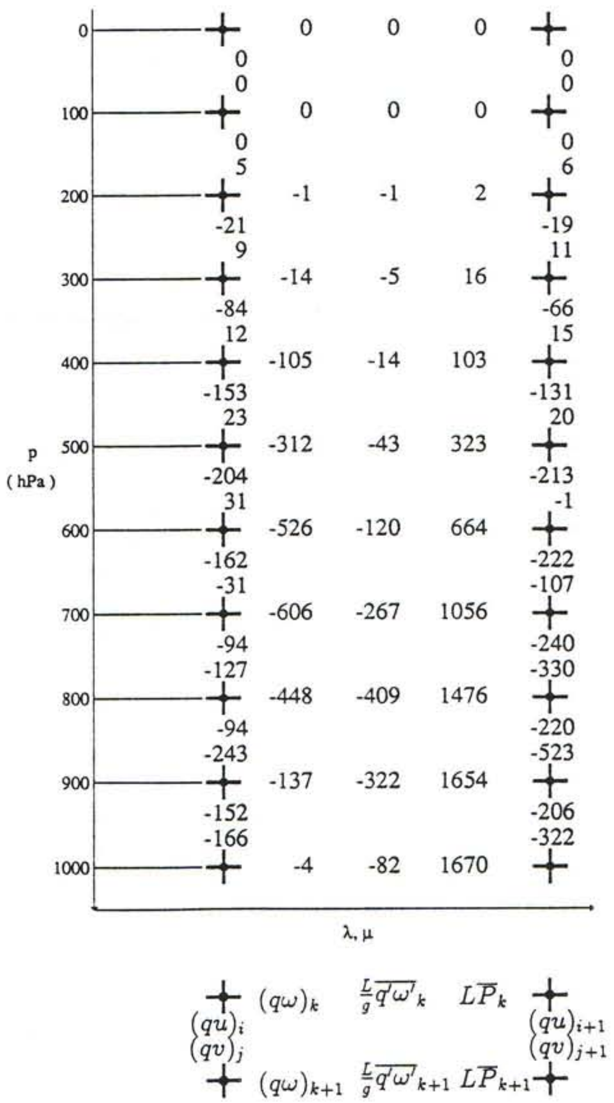

Fig. 4.4. Horizontal (gridscale) and vertical (both gridscale and sub-gridscale) fluxes across boundaries of all boxes of column SALZBURG (for position see Fig. 2.3) for 1 August 1991, 00GMT ± 6h, in units W/m²; sub-gridscale fluxes r, f are denoted consistent with eqs. (1.1), (1.2) whereas gridscale fluxes are denoted by abbreviations according to:

$(qu)_i$ stands for

$$L\frac{dp}{a\,g\,d\lambda}\int_{t=t_0}^{t_0+\Delta t}\int_{p=p_k}^{p_{k+1}}\int_{\mu=\mu_r}^{\mu_{r+1}}\left(\frac{qu}{\cos\phi}\right)_i d\mu\,dp\,dt \Big/ \int_{t=t_0}^{t_0+\Delta t}\int_{p=p_k}^{p_{k+1}}\int_{\mu=\mu_r}^{\mu_{r+1}} d\mu\,dp\,dt$$

$(qv)_j$ stands for

$$L\frac{dp}{a\,g\,d\mu}\cos\phi\int_{t=t_0}^{t_0+\Delta t}\int_{p=p_k}^{p_{k+1}}\int_{\lambda=\lambda_r}^{\lambda_{r+1}}(qv)_j\,d\lambda\,dp\,dt \Big/ \int_{t=t_0}^{t_0+\Delta t}\int_{p=p_k}^{p_{k+1}}\int_{\lambda=\lambda_r}^{\lambda_{r+1}} d\lambda\,dp\,dt$$

$(q\omega)_k$ stands for

$$L\frac{1}{g}\int_{t=t_0}^{t_0+\Delta t}\int_{\lambda=\lambda_r}^{\lambda_{r+1}}\int_{\mu=\mu_r}^{\mu_{r+1}}(q\omega)_k\,d\mu\,d\lambda\,dt \Big/ \int_{t=t_0}^{t_0+\Delta t}\int_{\lambda=\lambda_r}^{\lambda_{r+1}}\int_{\mu=\mu_r}^{\mu_{r+1}} d\mu\,d\lambda\,dt$$

Note that these represent components of 3D-gridscale moisture flux across respective faces of diagnostic boxes.

Abb. 4.4. Horizontale (skalige) und vertikale (sowohl skalige als auch subskalige) Flüsse durch Grenzflächen sämtlicher Boxen der Säule SALZBURG (zur Lokalisierung s. Abb. 2.3) vom 1. August 1991, 00GMT ± 6h, in W/m²; Bezeichnungen subskaliger Flüsse f und r konsistent mit Glgen. (1.1), (1.2), hingegen werden skalige Flüsse mit Abkürzungen bezeichnet gemäß:

$(qu)_i$ steht für

$$L\frac{dp}{a\,g\,d\lambda}\int_{t=t_0}^{t_0+\Delta t}\int_{p=p_k}^{p_{k+1}}\int_{\mu=\mu_r}^{\mu_{r+1}}\left(\frac{qu}{\cos\phi}\right)_i d\mu\,dp\,dt \Big/ \int_{t=t_0}^{t_0+\Delta t}\int_{p=p_k}^{p_{k+1}}\int_{\mu=\mu_r}^{\mu_{r+1}} d\mu\,dp\,dt$$

$(qv)_j$ steht für

$$L\frac{dp}{a\,g\,d\mu}\cos\phi\int_{t=t_0}^{t_0+\Delta t}\int_{p=p_k}^{p_{k+1}}\int_{\lambda=\lambda_r}^{\lambda_{r+1}}(qv)_j\,d\lambda\,dp\,dt \Big/ \int_{t=t_0}^{t_0+\Delta t}\int_{p=p_k}^{p_{k+1}}\int_{\lambda=\lambda_r}^{\lambda_{r+1}} d\lambda\,dp\,dt$$

$(q\omega)_k$ steht für

$$L\frac{1}{g}\int_{t=t_0}^{t_0+\Delta t}\int_{\lambda=\lambda_r}^{\lambda_{r+1}}\int_{\mu=\mu_r}^{\mu_{r+1}}(q\omega)_k\,d\mu\,d\lambda\,dt \Big/ \int_{t=t_0}^{t_0+\Delta t}\int_{\lambda=\lambda_r}^{\lambda_{r+1}}\int_{\mu=\mu_r}^{\mu_{r+1}} d\mu\,d\lambda\,dt$$

Man beachte, daß diese Flüsse die Komponenten des 3D-skaligen Feuchteflusses durch die entsprechenden Grenzflächen der diagnostischen Box repräsentieren.

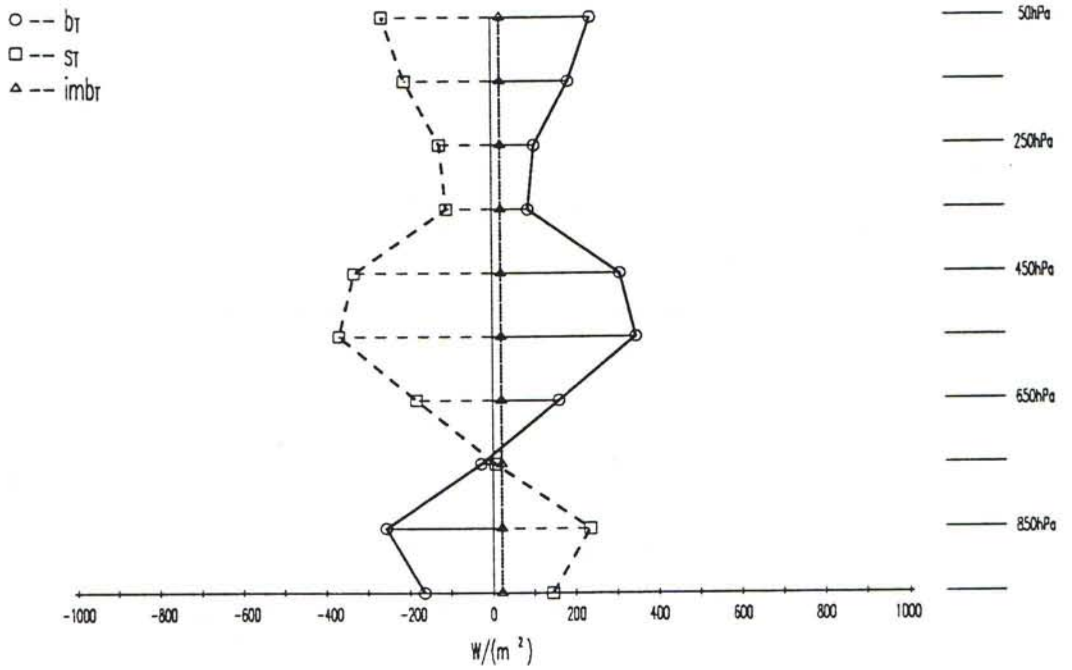

Fig. 4.5. Vertical profiles of b_T, s_T and imb_T in column SALZBURG (for position see Fig. 2.3) for 1 August 1991, 00GMT ± 6h, in units W/m²; values given by symbols are centered in middle of corresponding diagnostic box (e.g. value of b_T in 450 hPa represents the 400—500 hPa layer).

Abb. 4.5. Vertikalprofile von b_T, s_T und imb_T der Säule SALZBURG (zur Lokalisierung s. Abb. 2.3) vom 1. August 1991, 00GMT ± 6h, in W/m²; durch Symbole gekennzeichnete Werte sind in der Mitte der entsprechenden diagnostischen Box angegeben (z. B., Wert von b_T in 450 hPa repräsentiert die 400—500 hPa Schicht).

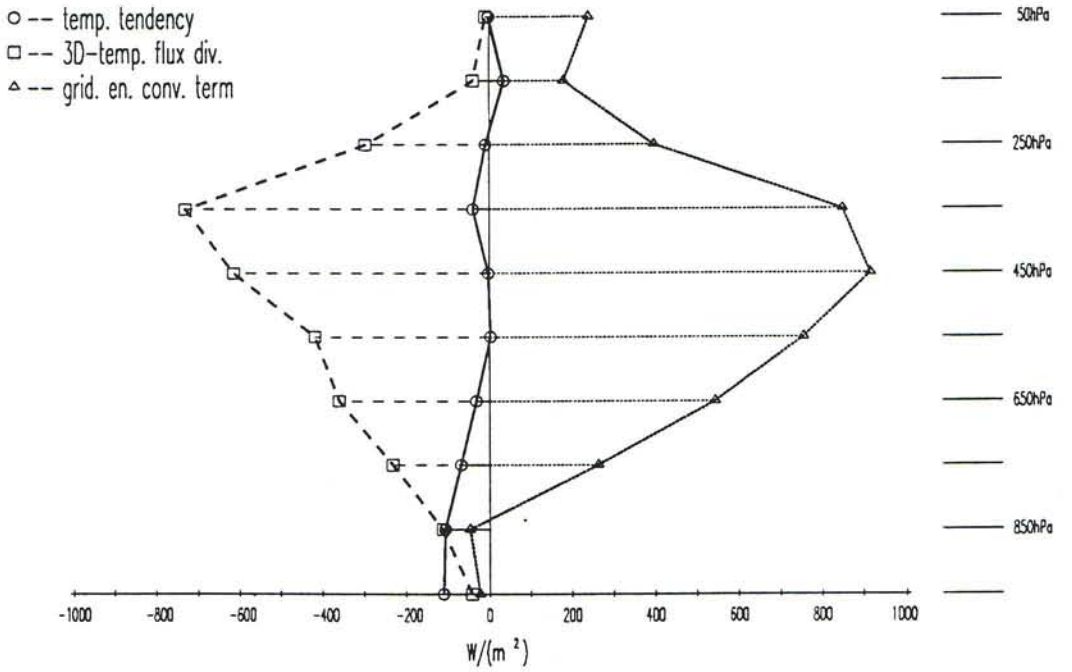

Fig. 4.6. Components of gridscale T-budget in column SALZBURG (for position see Fig. 2.3) for 1 August 1991, 00GMT ± 6h, in units W/m²; values given by symbols are centered in middle of corresponding diagnostic box (e.g., value of $c_p \frac{\partial T}{\partial t}$ in 450 hPa represents 400—500 hPa layer).

Abb. 4.6. Komponenten des skaligen T-Budgets der Säule SALZBURG (zur Lokalisierung s. Abb. 2.3) vom 1. August 1991, 00GMT ± 6h, in W/m²; durch Symbole gekennzeichnete Werte sind in der Mitte der entsprechenden diagnostischen Box angegeben (z. B., Wert von $c_p \frac{\partial T}{\partial t}$ in 450 hPa repräsentiert die 400—500 hPa Schicht).

ing to our error model, the column imbalance is assumed constant in the vertical resulting in a mean box imbalance of $imb_T = 21$ W/m². Again, this relatively low figure lends credence to the vertical profile of the signal s_T which is positive in the lowest layer and negative above 700 hPa. While the moisture budget is practically zero above 300 hPa (Fig. 4.2) the temperature budget shows values exceeding 200 W/m² per 100 hPa even in the stratosphere layer.

Opposite to the q-budget, the gridscale T-budget cannot be readily interpreted with the familiar concept of *divergence* and *convergence*. The reason is demonstrated in Fig. 4.6 by the decomposition of the T-budget according to [compare eq. (2.2) and Fig. 2.1]:

$$b_T = \underbrace{c_p \frac{\partial T}{\partial t}}_{\text{tendency}} + \underbrace{c_p \nabla \cdot TV + c_p \frac{\partial T\omega}{\partial p}}_{\text{3D - divergence}} \underbrace{- c_p \frac{\kappa}{p} T\omega}_{\text{energy conversion}} + g \frac{\partial R}{\partial p}. \qquad (4.1)$$

Neither the tendency nor the radiation flux divergence has a governing influence. It is the balance between the 3D-temperature flux divergence and the energy conversion term which controls the budget. The latter two terms compensate each other to a considerable degree; however, the energy conversion term eventually determines the sign of b_T throughout most of the column. The plots for the T-budget that would be equivalent to Figs. 4.3, 4.4 are not repoduced. It may suffice to note that the horizontal gridscale T-fluxes are about one order of magnitude larger than their q-counterparts; also, the vertical gridscale T-flux is much larger than w. This supports the results of EMEIS (1985) who has discussed this point in some detail.

In Fig. 4.7, equivalently to Fig. 4.6, the sub-gridscale signal is decomposed according to [compare eq. (2.2) and Fig. 2.1]:

$$s_T = \underbrace{g \frac{\partial w}{\partial p}}_{\text{heat flux div.}} \underbrace{- g \frac{\kappa}{p} w}_{\text{subsc. en. conv.}} \underbrace{- g \frac{\partial r}{\partial p}}_{\text{rain flux div.}}. \qquad (4.2)$$

Opposite to the gridscale energy conversion term its sub-gridscale equivalent has a minor influence upon the signal. Rather, s_T is in the upper atmosphere governed by the heat flux divergence (which actually is a convergence). Below about 300 hPa the divergences of w and of r balance each other; note the negative sign in front of $\partial r/\partial p$. The result of this balance is such that in the middle troposphere the rain flux divergence is the controlling quantity and causes negative s_T while in the lowest tropospheric layers 800—1000 hPa the heat flux divergence overcompensates the rain influence and explains the positive s_T. The large sub-gridscale

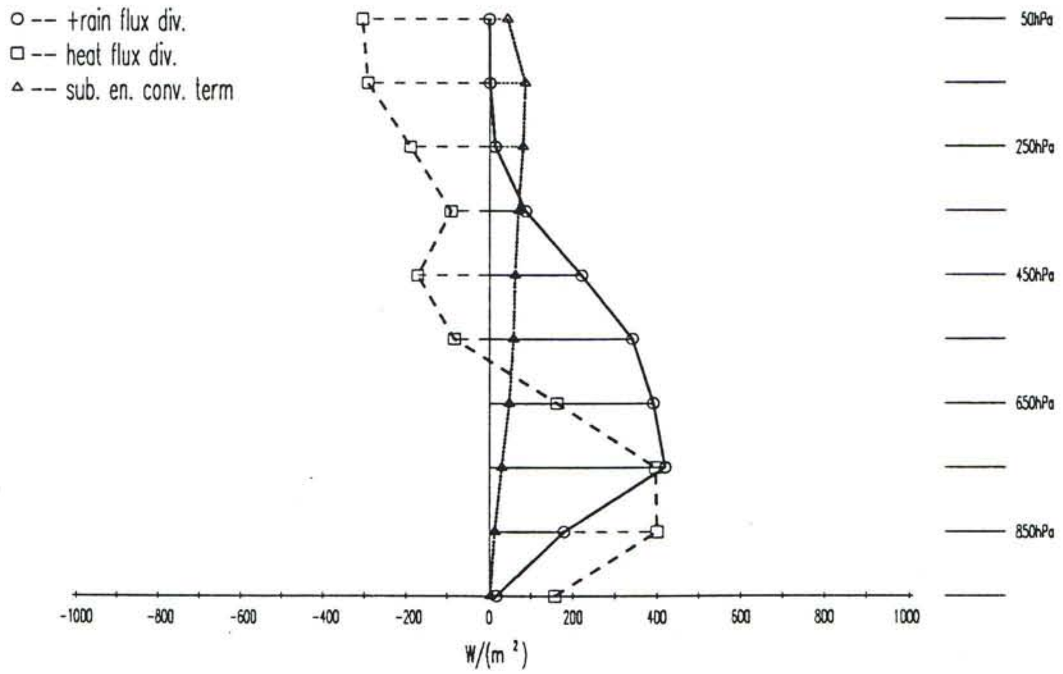

Fig. 4.7. Components of sub-gridscale T-budget in column SALZBURG (for position see Fig. 2.3) for 1 August 1991, 00GMT ± 6h, in units W/m²; values given by symbols are centered in middle of corresponding diagnostic box (e.g., value of $g \frac{\partial w}{\partial p}$ in 450 hPa represents 400—500 hPa layer; note: plotted is $+ g \frac{\partial r}{\partial p}$).

Abb. 4.7. Komponenten des subskaligen T-Budgets der Säule SALZBURG (zur Lokalisierung s. Abb. 2.3) vom 1. August 1991, 00GMT ± 6h, in W/m²; durch Symbole gekennzeichnete Werte sind in der Mitte der entsprechenden diagnostischen Box angegeben (z. B., Wert von $g \frac{\partial w}{\partial p}$ in 450 hPa repräsentiert die 400—500 hPa Schicht; beachte: dargestellt ist $+ g \frac{\partial r}{\partial p}$).

heat flux divergence in the lower troposphere (400 W/m² per 100 hPa) causes the strong upward w.

This leads us back to Fig. 4.1 and to the remarkable sub-gridscale upward fluxes f and w. These fluxes represent convective activity which reaches high up even into the stratosphere; the maximum is attained in the middle of the troposphere. It is this convective activity which, together with the gridscale moisture budget, explains the strong rain flux. The SALZBURG column is the most prominent example for this configuration; it is representative also for its adjacent columns. We have chosen the SALZBURG column for the present detailed discussion not only because it represented the peak of the rain episode but also because it serves as a fine example to demonstrate the power of DIAMOD.

5. Results for Central Europe

DIAMOD is a diagnostic model for *one atmospheric column*. There is no interaction with adjacent columns in contrast to using the budget equations in the forecast mode. Each column is diagnostically evaluated independent upon any explicit information from the next column. There is, however, an indirect coupling through the analysed input data. For example, a zonal moisture flux across a vertical face separating two columns obviously enters the budget of both columns and thus influences both.

After having considered the SALZBURG column individually we shall now consider the geographical pattern of an array of many neighbouring columns over Europe. In the present implentation of DIAMOD each one of the 32 × 32 columns of Fig. 2.3 is routinely evaluated. For the purpose of this section we shall focus on the rectangle sketched in Fig. 2.3 comprising 14 × 14 columns.

5.1 *Vertical sub-gridscale fluxes over Central Europe*

Fig. 5.1 shows vertical profiles of the sub-gridscale fluxes r, f and w in each of the 14 × 14 diagnostic columns. The profiles are plotted at about the geographical location of each column. The region of heavy surface rain that extends deeply upward into the troposphere is clearly depicted; it is centered over north central Austria. The strong upward fluxes of f and w over this region are likewise visible. This indicates that the rain area, at least under these circumstances, is characterized both by strong free atmosphere precipitation

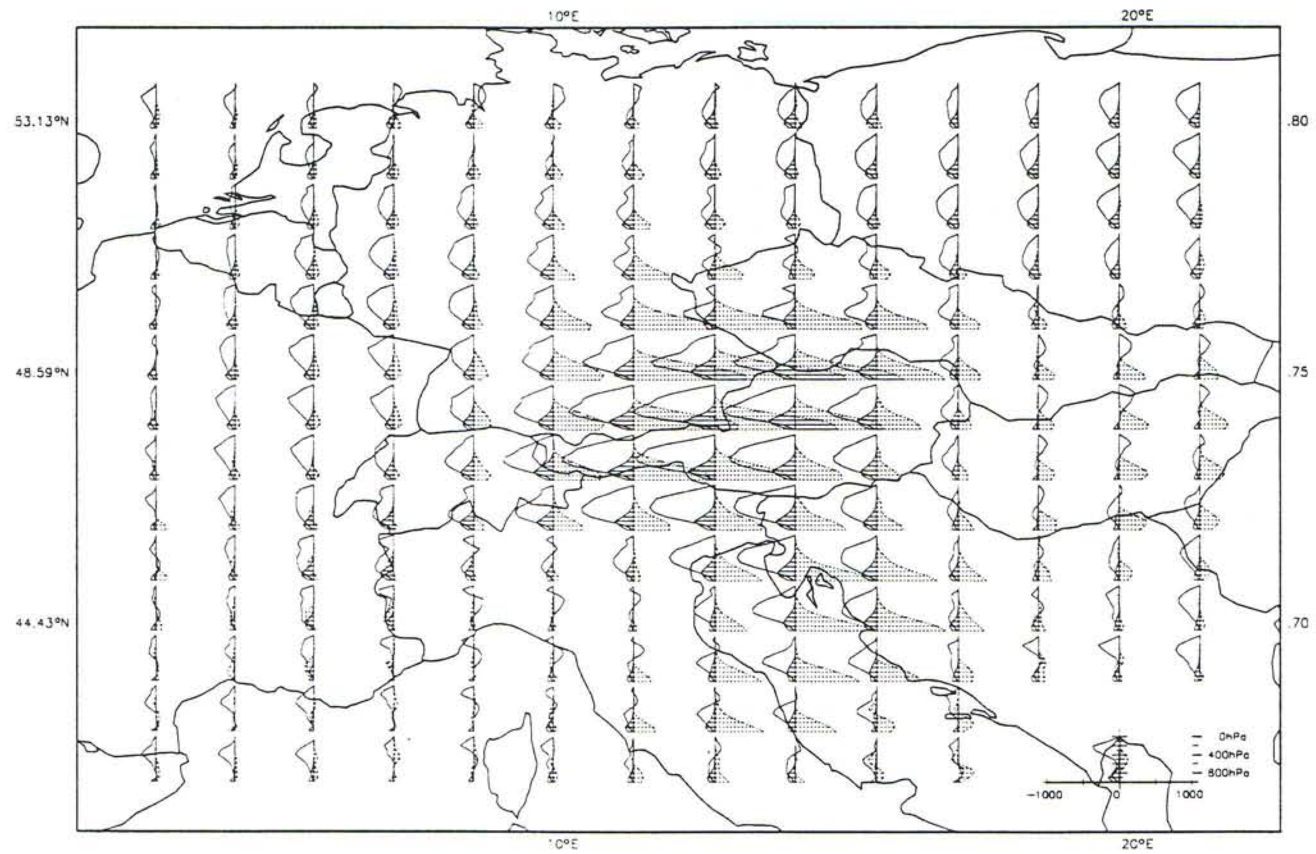

Fig. 5.1. Array of 14 × 14 diagnostic columns over Central Europe showing vertical profiles r, f and w for 1 August 1991, 00GMT ± 6h, in units W/m² (compare Fig. 2.3); scale as indicated; each individual profile is arranged similarly to Fig. 4.1; specifically, dashed, hatched and blank profiles denote profiles of r, f and w, respectively.

Abb. 5.1. Vertikalprofile von r, f und w von 14 × 14 diagnostischen Säulen über Mitteleuropa vom 1. August 1991, 00GMT ± 6h, in W/m² (vgl. Abb. 2.3); Maßstab angegeben; Anordnung der Einzelprofile entspricht Abb. 4.1; speziell: strichlierte, schraffierte und nicht ausgefüllte Profile bezeichnen Profile von r, f und w.

as well as by strong upward convection. The maxima of f over the rain area are located in the 800 hPa-level with about —400 W/m² while the maxima of w can be found in 600 hPa with values of up to —1100 W/m². All sub-gridscale fluxes exhibit a strong horizontal gradient towards the north of Italy, towards Bohemia and towards the west of Hungary.

The characteristics of the profiles outside the area of maximum precipitation are quite different from the ones inside. We may distinguish between atmospheric conditions with little or no rain but sizeable convection (northern France; Poland) and those with sizeable rain but little or no upward convection (eastern Hungary). The France/Poland profiles of w peak in levels 300 to 400 hPa, but are much lower in value than over the rain maximum. The Hungarian profiles indicate a truly large-scale rain with no appreciable convective activity.

5. 2 *Budget components over Central Europe*

Vertical profiles of the gridscale moisture budget are reproduced in Fig. 5.2. We may distinguish the following different types:

1. strongly negative b_q with almost constant values up to the upper troposphere (southern Germany);
2. negative b_q with a pronounced peak in the 700—800 hPa-layer (Hungary, extending into Czechoslovakia);
3. insignificant or weakly positive b_q (France, Poland); and
4. significantly positive b_q (northern Mediterranean).

We shall try to compare these types with the precipitation and convection characteristics that have been found in Section 5.1. It will certainly not be possible to get, by combining the rough classification suggested by Figs. 5.1, 5.2, a complete characterization of the budget types. Some gross features seem however to emerge. They can be sketched as follows:

I. The heavy rain area (Fig. 5.1) corresponds with budget category 1) as far as most of Austria, southern Germany and western Czechoslovakia is concerned.

II. Similar to I), the rain area over central and eastern Hungary corresponds quite well to budget category 2). The difference to I) is that there is no pronounced upward convection (see Fig. 5.1) implying that the observed rain must be large-scale generated. In summary, the moisture budget categories 1), 2) seem to be relevant for sizeable area precipitation.

III. In areas of little or no observed surface rain (France, Poland), the budget category 3) is correlated with sizeable convective activity (see Fig. 5.1).

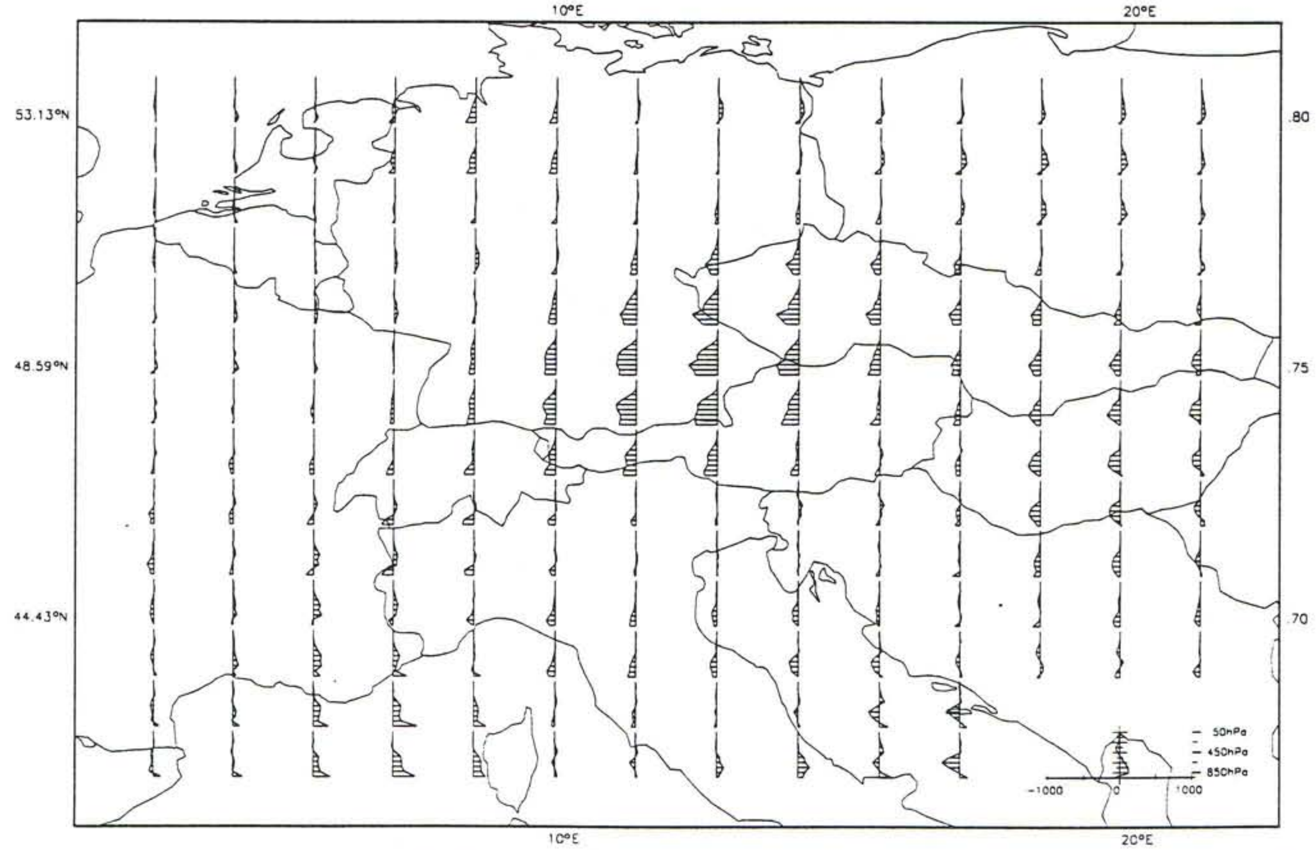

Fig. 5.2. Array of 14 × 14 diagnostic columns over Central Europe showing b_q for 1 August 1991, 00GMT ± 6h, in units W/m² (compare Fig. 2.3); scale as indicated.

Abb. 5.2. b_q von 14 × 14 diagnostischen Säulen über Mitteleuropa vom 1. August 1991, 00GMT ± 6h, in W/m² (vgl. Abb. 2.3); Maßstab angegeben.

Let us next consider the errors of the budgets. Fig. 5.3 shows the vertical mean box imbalances $\overset{\infty}{\mathrm{imb}}_q$ (left symbolic column at each respective geographical location) and $\overset{\infty}{\mathrm{imb}}_T$ (right column). They have values from zero to more than 120 W/m². In order to get the respective column imbalance just multiply by 10. As has been discussed in Section 2.2, both vertical mean imbalances can be considered observed.

While Fig. 5.3 does hardly allow for a detailed classification, we can easily distinguish between the following extremes:

a. both imbalances small (Central Austria around Salzburg, Central Germany, various other locations including eastern Hungary); and
b. one or both imbalances large (northern Adriatic and Yugoslavia, Switzerland, northern Mediterranean).

We have tried to define quantitative limits for *small* (smaller than about 20 W/m²) and *large* (larger than about 100 W/m²) imbalances but are not satisfied with this or any similar choice. Nevertheless, there clearly exists a pronounced difference in the imbalance of, for example, the columns SALZBURG (small) and PULA (large). Thus for the time being we shall adopt these two categories.

The budget/rain categories I and II just discussed fall into imbalance category a). The rain maximum around SALZBURG and the weaker but still significant rain maximum over eastern Hungary are represented by columns with small imbalances. It is over these areas where the results of DIAMOD deserve maximum credence.

The opposite applies to columns with category b). Areas with high analysed surface rain, combined with high imbalances, cast doubts upon the consistency between rain field and free atmosphere data. An example can be seen in the northern parts of the Adriatic and Yugoslavia. Fig. 5.1 shows considerable rain over this area, however without a significant b_q (Fig. 5.2). Most of the rain signal can be explained by the imbalance (Fig. 5.3, both imbalances large and of opposite sign). We may at this stage further subclassify the imbalance category b) as follows: if imb_q is negative (positive) the analysed rain is overestimated (underestimated). This becomes clearer from eq. (2.1). The rain flux divergence is in general positive throughout the column. For the case of vanishing gridscale moisture budget and sub-gridscale moisture flux divergence a (positive) rain flux divergence caused by an overestimated analysed rain can only be balanced by a negative imb_q.

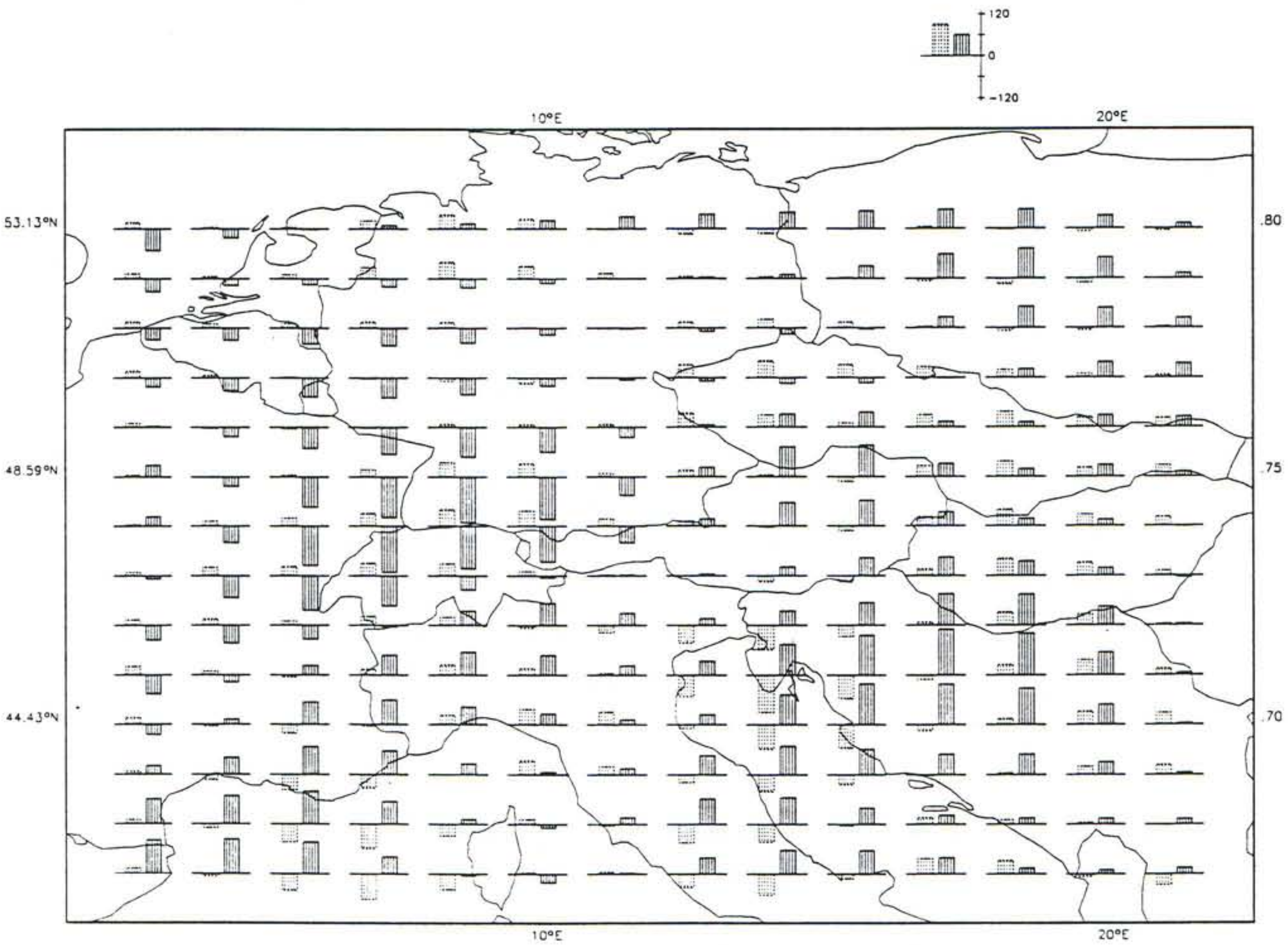

Fig. 5.3. $\overset{\infty}{\mathrm{imb}}_q$ (dashed) and $\overset{\infty}{\mathrm{imb}}_T$ (solid) for array of 14 × 14 diagnostic columns over Central Europe for 1 August 1991, 00GMT ± 6h, in units W/m² (compare Fig. 2.3); scale as indicated.

Abb. 5.3. $\overset{\infty}{\mathrm{imb}}_q$ (strichliert) und $\overset{\infty}{\mathrm{imb}}_T$ (durchgezogen) von 14 × 14 diagnostischen Säulen über Mitteleuropa vom 1. August 1991, 00GMT ± 6h, in W/m² (vgl. Abb. 2.3); Maßstab angegeben.

What ist the reason for this overestimation in the Adriatic-Yugoslavian area? It appears that probably both the atmospheric analysis and the rain measurements were correct but the rain analysis was not representative. This interpretation is supported by the IR-satellite image for this date (not shown). The satellite picture indicates a small convective cell over the south of Istria moving slowly eastward. The consequence is: On the one hand the SYNOP rain information is spread out over a large area by our objective rain analysis method with the result that the analysed rain is exaggerated; on the other hand, since the scale of the convective cell is so small the ECMWF-analysis, quite properly, does not resolve it. In this case the error of the rain analysis, since it acts into opposite directions in the heat budgets, generates sizeable imbalances of different sign.

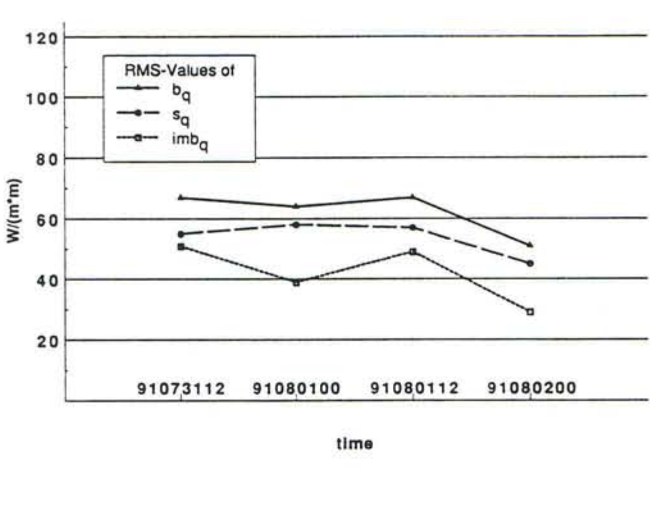

Fig. 5.4. Comparison of b_q, s_q and imb_q (top, compare Fig. 5.2, 5.3) and of b_T, s_T and imb_T (bottom) for two successive days in units W/m²; data are rms-averaged over 14 × 14 × 10 diagnostic boxes; given values are centered at time indicated (± 6h).

Abb. 5.4. Vergleich von b_q, s_q und imb_q (oben, vgl. Abb. 5.2, 5.3) und von b_T, s_T und imb_T (unten) für zwei aufeinanderfolgende Tage in W/m²; Daten sind über 14 × 14 diagnostische Säulen rms-gemittelt; dargestellte Werte sind um angegebenen Zeitpunkt zentriert (± 6h).

The category 4) with consistently positive b_q represents budgets that are dubious *a priori* in the extratropics. Fig. 5.3 shows that the columns concerned (e.g., the area in the northwestern Mediterranean) also have large imbalances of category b). Thus we shall not have too much credence in the sub-gridscale fluxes (Fig. 5.1) over this area. After all, there are no direct surface rain measurements over sea so that the input data of PREC are an artificial product of our analysis scheme over the Mediterranean.

Fig. 5.4 summarizes the budget terms, averaged over the inset of Fig. 2.3, in their time development during the rain episode. The components of the heat budget are regularly larger than those of the moisture budget; this had already been found by EMEIS (1985a). The main reason for this seems to be that the individual fluxes (both in horizontal and vertical directions) in the heat budget are larger than they are in the moisture budget. The ω-field that enters the adiabatic term is limited in accuracy and tends to cause relatively high analysis sensitivity of b_T and consequently relatively large imb_T. The mean imb_q over the 4 days of Fig. 5.4 is 42 W/m², the mean imb_T is 57 W/m².

The signal of both budgets is in all cases higher than the respective imbalance. This suggests that DIAMOD tends to separate the signal from the error to the extent that it makes sense to physically interprete the signal, specifically the derived sub-gridscale fluxes.

6. Physical mechanisms

In this section we shall try to categorize the physical mechanisms that may be at work during this meteorological episode. First attempts into this direction have been made by EMEIS (1985a, 1985b) who attributed specific vertical flux profile types to certain areas of an ideal midlatitude cyclone. For example, EMEIS suggested that in the warm sector the sub-gridscale fluxes are minor because the upward motion is gridscale; further, that the upward moisture flux has its maximum at the cold front; and finally, that the maximum dry enthalpy flux is found in the convectively active zone behind the cold front.

For the present case these types do not apply because, as we have indicated (Section 3), there are no fronts; rather, the situation is more tropical in character. Further, we shall start the subsequent discussion with the *caveat* in mind that the interpretation of an observed budget cannot yield a unique distinction between cause and effect; the following categorization will thus be preliminary. We shall use for our purpose some selected columns. Their location is given in Fig. 2.3. The column SALZBURG is also a member of this ensemble. The columns selected are representative for others in their vicinity.

6.1 *Columns with significant budget: Large-scale rain*

Fig. 6.1 shows the profiles for fluxes and moisture budget components within the column FREISTADT. This column is located in the center of the rain maximum on 2 August, just northeast of SALZBURG. The surface rain amounts to 872 W/m², the imbalances are small, and there are strong horizontal fluxes (not shown) along with insignificant convective fluxes. This is indeed the main difference to SALZBURG (see Figs. 4.1, 4.2). We consider this as representative for the ideal case of a non-convective rain production.

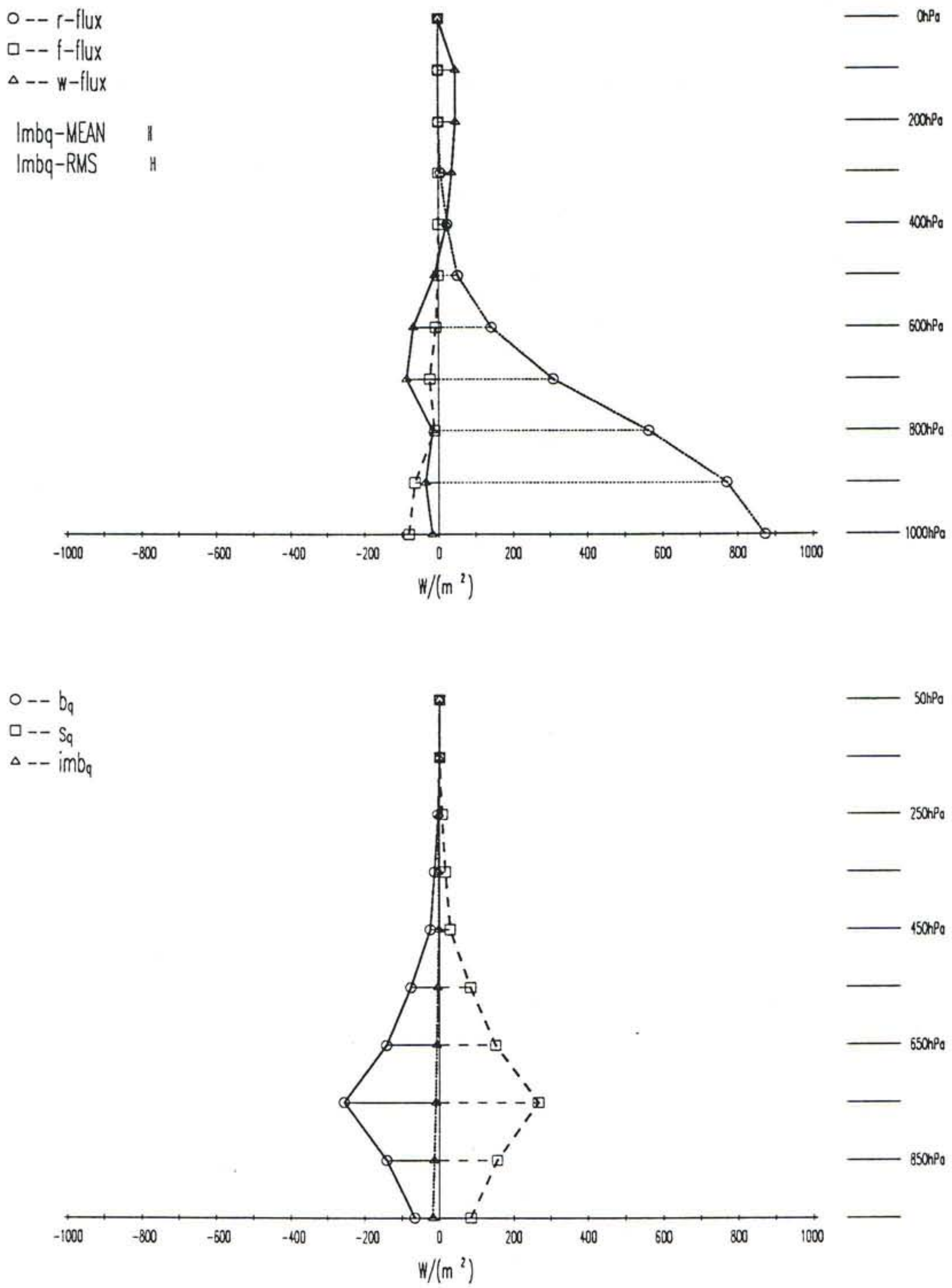

Fig. 6.1. Vertical profiles of r, f and w (top) and of b_q, s_q and imb_q (bottom) in column FREISTADT (for position see Fig. 2.3) for 2 August 1991, 00GMT ± 6h in units W/m²; meaning of symbols same as in Fig. 4.1 and Fig. 4.2 respectively.

Abb 6.1. Vertikalprofile von r, f und w (oben) und von b_q, s_q und imb_q (unten) der Säule FREISTADT (zur Lokalisierung s. Abb. 2.3) vom 2. August 1991, 00GMT ± 6h, in W/m²; Bedeutung der Symbole wie in Abb. 4.1 und in Abb. 4.2 angegeben.

6.2 *Columns with insignificant budget: Convective rain*

The opposite ideal case would be precipitation of purely convective origin, implying that no large-scale convergence is present. This requires in the ideal case a vanishing moisture budget (category 3). We have found various instances with practically zero moisture budget (compare Fig. 5.2). These can be further subdivided as follows.

6.2.1 The zero case: Convection without rain

Fig. 6.2 shows the profiles for fluxes and buget components within the column MILANO. All moisture budget components are indeed quite inactive. However, dictated by the heat budget (not shown), there is sizeable convection; w across 400 hPa exceeds 400 W/m². In accord with the dry atmosphere over northern Italy in this case, there is very little moisture flux and practically no rain.

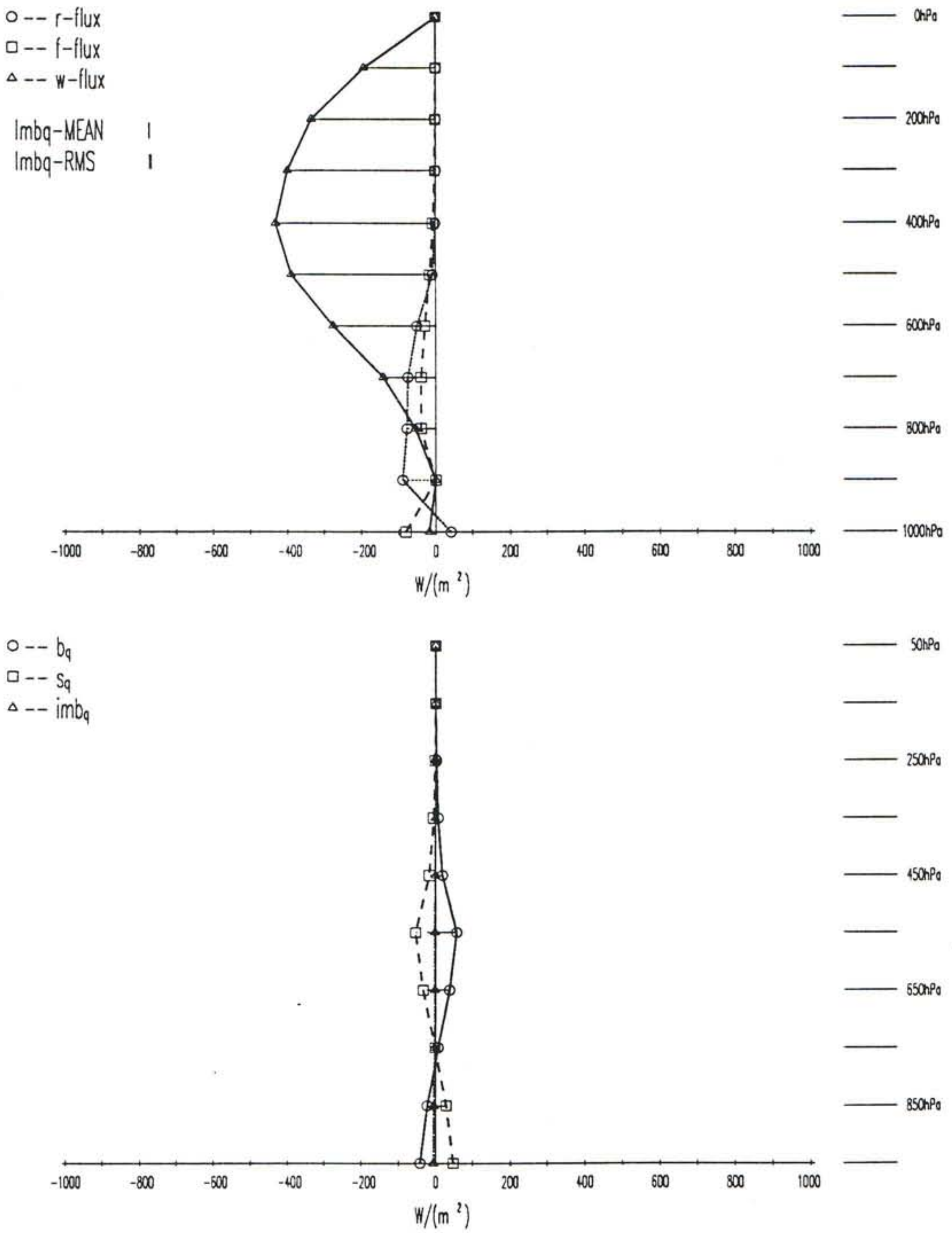

Fig. 6.2. Same as Fig. 6.1, but for column MILANO for 1 August 1991, 12GMT ± 6h.

Abb. 6.2. Wie Abb. 6.1, aber für Säule MILANO vom 1. August 1991, 12GMT ± 6h.

6.2.2 The pure case: Convection with rain

Fig. 6.3 shows the profiles for fluxes and moisture budget components within the column LJUBLJANA. The moisture budget is totally inactive in all its components. The observed rain (77 W/m^2) is weak but significant. Its divergence is balanced by the sub-gridscale moisture flux divergence. The surface evaporation is transported upwards, the moisture flux peaks across 800 hPa and converges higher up. This convection is supported by the sub-gridscale heat flux which is even stronger and reaches up into the upper troposphere. We may consider this a pure tropical case in the sense that the evaporating rain precipitates at the same geographical location without a significant horizontal moisture flux convergence.

This interpretation of the column LJUBLJANA is consistent with the synoptic situation as discussed in Section 3.1.

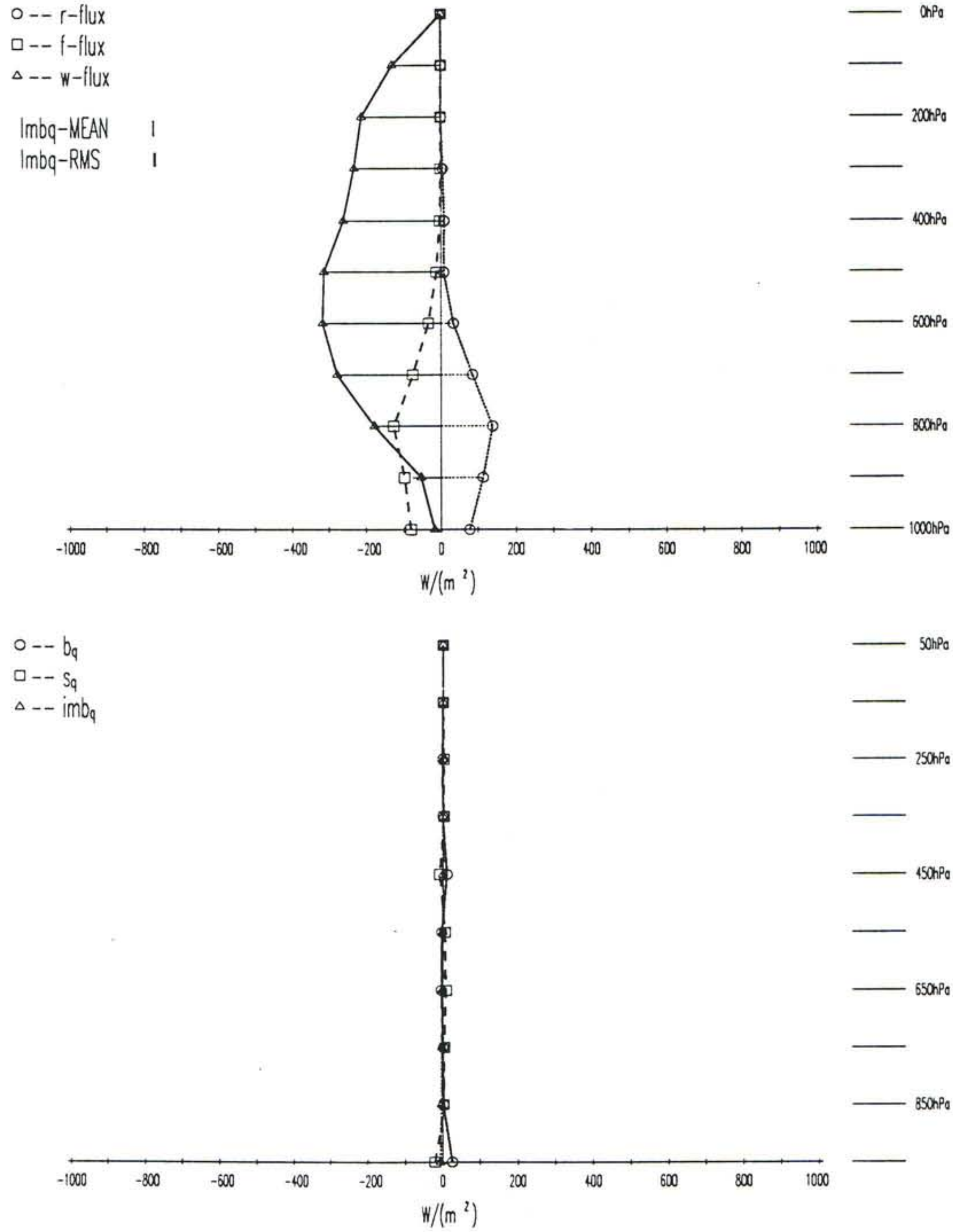

Fig. 6.3. Same as Fig. 6.1, but for column LJUBLJANA for 2 August 1991, 00GMT ± 6h.

Abb. 6.3. Wie Abb. 6.1, aber für Säule LJUBLJANA vom 2. August 1991, 00GMT ± 6h.

6.2.3 The dubious case: Convection and rain, but high error

Fig. 6.4 shows the profiles for fluxes and moisture budget components within the column PULA. This case has already been discussed in Section 5. While the air mass is probably much the same as in Fig. 6.3, the analysed rain seems to be overestimated as suggested by the size of imb_q. This causes doubtful signals s_q and s_T and consequently an overestimated convection.

6.3 *The SALZBURG column: Large-scale plus convective rain*

The SALZBURG column has already been discussed above; the figure equivalent to the previous 4 figures has been presented in Figs. 4.1, 4.2.

At first glance it may seem that Figs. 4.1, 6.4a are governed by similar physical mechanisms because the vertical flux profiles in both look quite similar (note, however, the

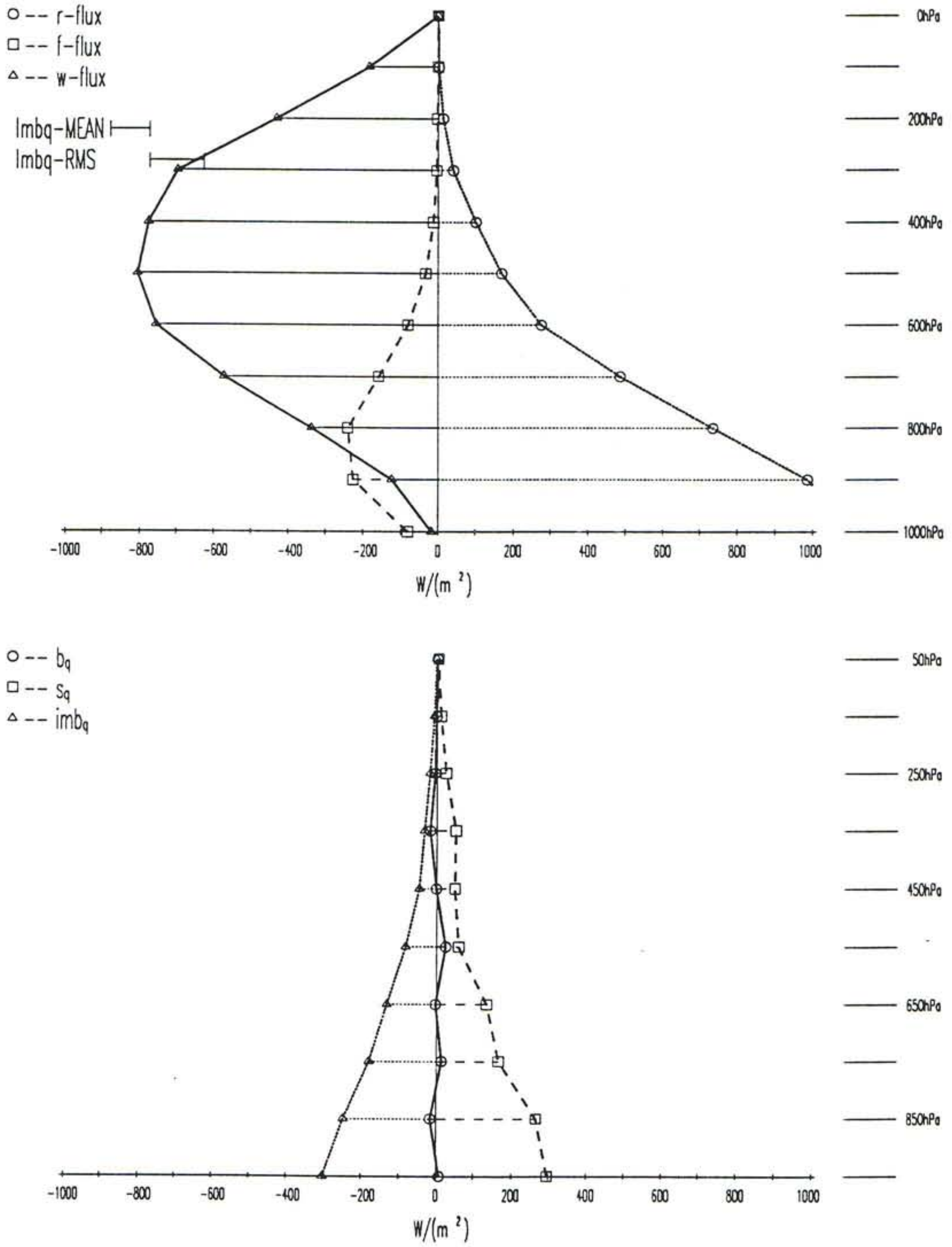

Fig. 6.4. Same as Fig. 6.1, but for column PULA for 1 August 1991, 00GMT ± 6h.

Abb. 6.4. Wie Abb. 6.1, aber für Säule PULA vom 1. August 1991, 00GMT ± 6h.

different scales of the respective figures). The difference between both is that SALZBURG (Fig. 4.1) has low imbalance and PULA (Fig. 6.4a) has high imbalance. Thus similar profiles of sub-gridscale fluxes must be considered in the light of the column imbalance. A column with insignificant budget but high imbalance has its signal controlled by the imbalance; this signal along with its derived fluxes must be considered with caution.

As mentioned before, SALZBURG is unique in that it combines the gridscale and the sub-gridscale contributions on basis of quite small imbalances. While a strongly negative b_q causes rain, a strongly negative $b_q + b_T$ causes convection (see also Part II). Both conditions are met in the SALZBURG column.

6.4 *Large-scale vs small-scale rain in ECMWF-forecasts*

We want to consider the precipitation forecast of the ECMWF for the first day of August in order to compare it with our diagnosed rain pattern (Fig. 3.5).

The ECMWF 36h-forecast for 1 August 1991 is reproduced in Fig. 6.5. Fig. 6.5a shows total rain, Fig. 6.5b large-scale and Fig. 6.5c small-scale rain. Comparing Fig. 6.5a with 3.5a it is evident that the total rain is considerably underestimated in the forecast. For example, the analysed rain over western Russia is more than an order of magnitude larger than its forecast equivalent. The net underprediction amounts to a factor of about 3 as can be seen from the statistics (mean: ECMWF: 26 W/m², analysed: 94 W/m²; rms: ECMWF: 94 W/m², analysed: 242 W/m²).

Nevertheless, the ECMWF-forecast of the location of the rain maximum over Austria is quite good. Further, according to Figs. 6.5b, 6.5c, the forecast rain is mainly on the small-scale.

Our analysis does not yield different rain types. In contrast to the ECMWF model we diagnose only one rain and cannot tell whether r(p) is large-scale or small-scale. However, we can tell if there is convection, and how much. Fig. 6.6 shows that there was indeed considerable convection in the Salzburg area with upward h-fluxes exceeding 1200 W/m². This at first glance tends to support the ECMWF-forecast of Fig. 6.5c.

What further information does the moisture budget provide in order to decide if a diagnosed rain is of convective or non-convective origin? As suggested in the Introduction,

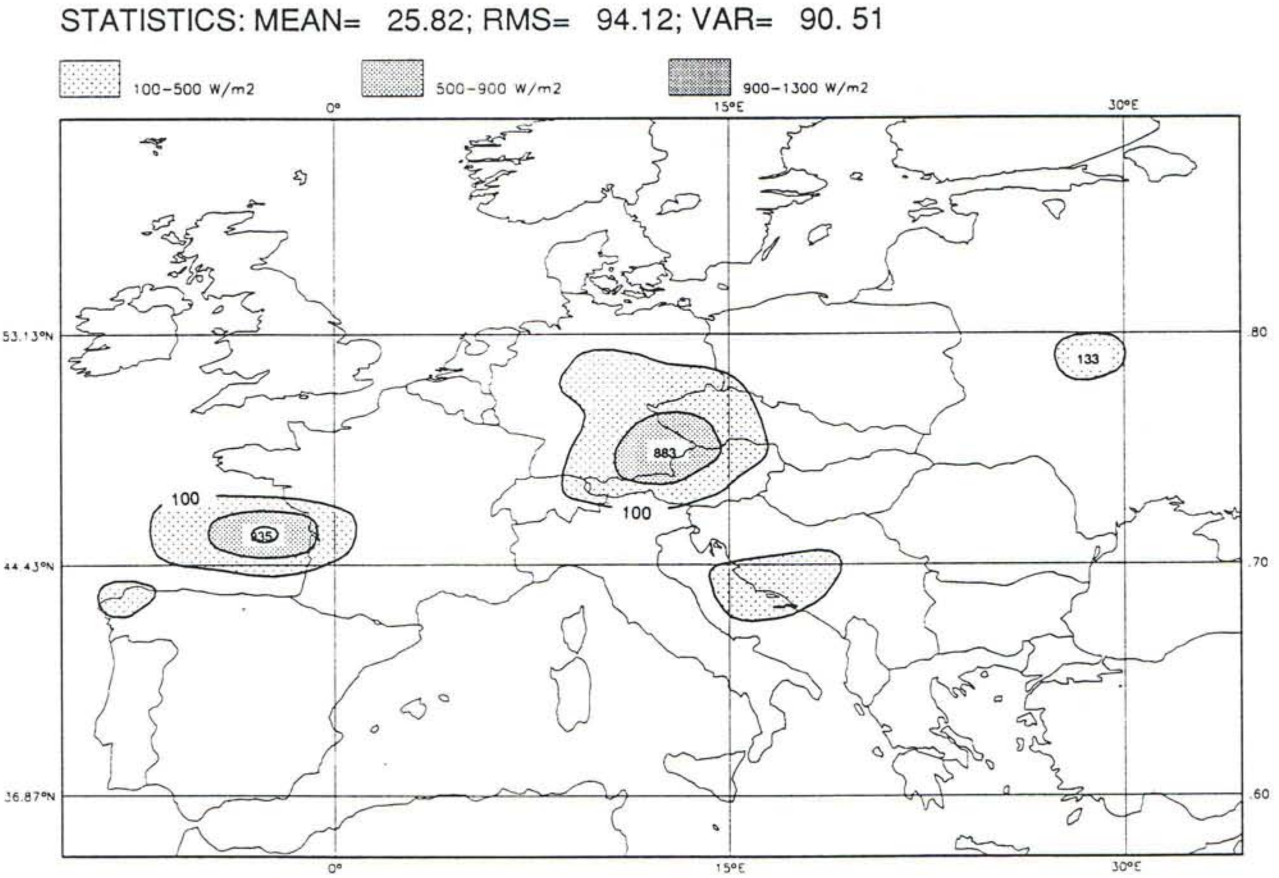

Fig. 6.5. ECMWF forecast for a) total (= large-scale + small-scale), b) large-scale and c) small-scale precipitation for 1 August 1991, 00GMT ± 6h in units W/m²; contour interval 400 W/m²; contour min value is 100 W/m² ≈ 1.7 mm/12h; forecast starts on 30 July 1991, 12GMT.

Abb. 6.5. Vorhersage des a) totalen (= large-scale + small-scale), des b) large-scale und des c) small-scale Niederschlages des EZMW vom 1. August 1991, 00GMT ± 6h, in W/m²; Konturintervall 400 W/m²; Vorhersage startet am 30. Juli 1991, 12GMT.

STATISTICS: MEAN= 8.02; RMS= 28.62; VAR= 27. 47

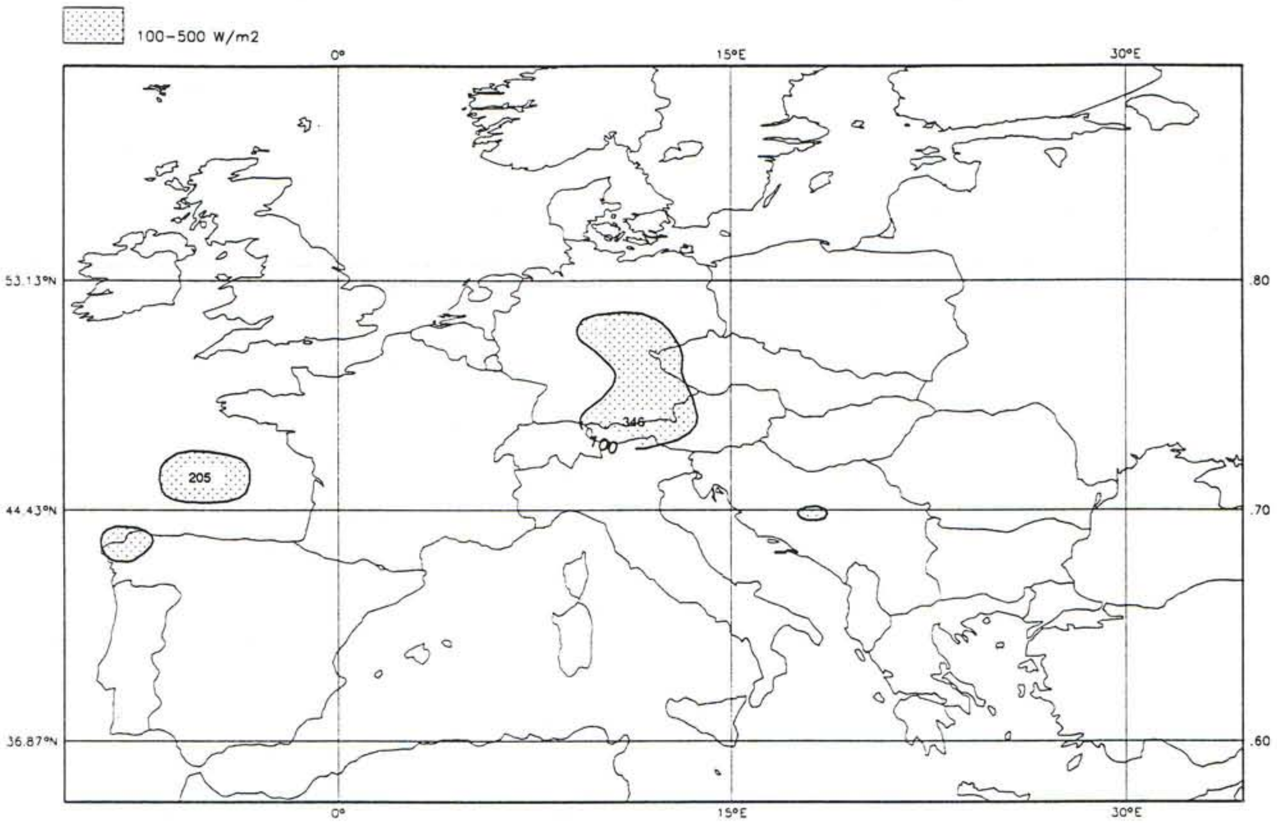

STATISTICS: MEAN= 17.80; RMS= 76.06; VAR= 73. 95

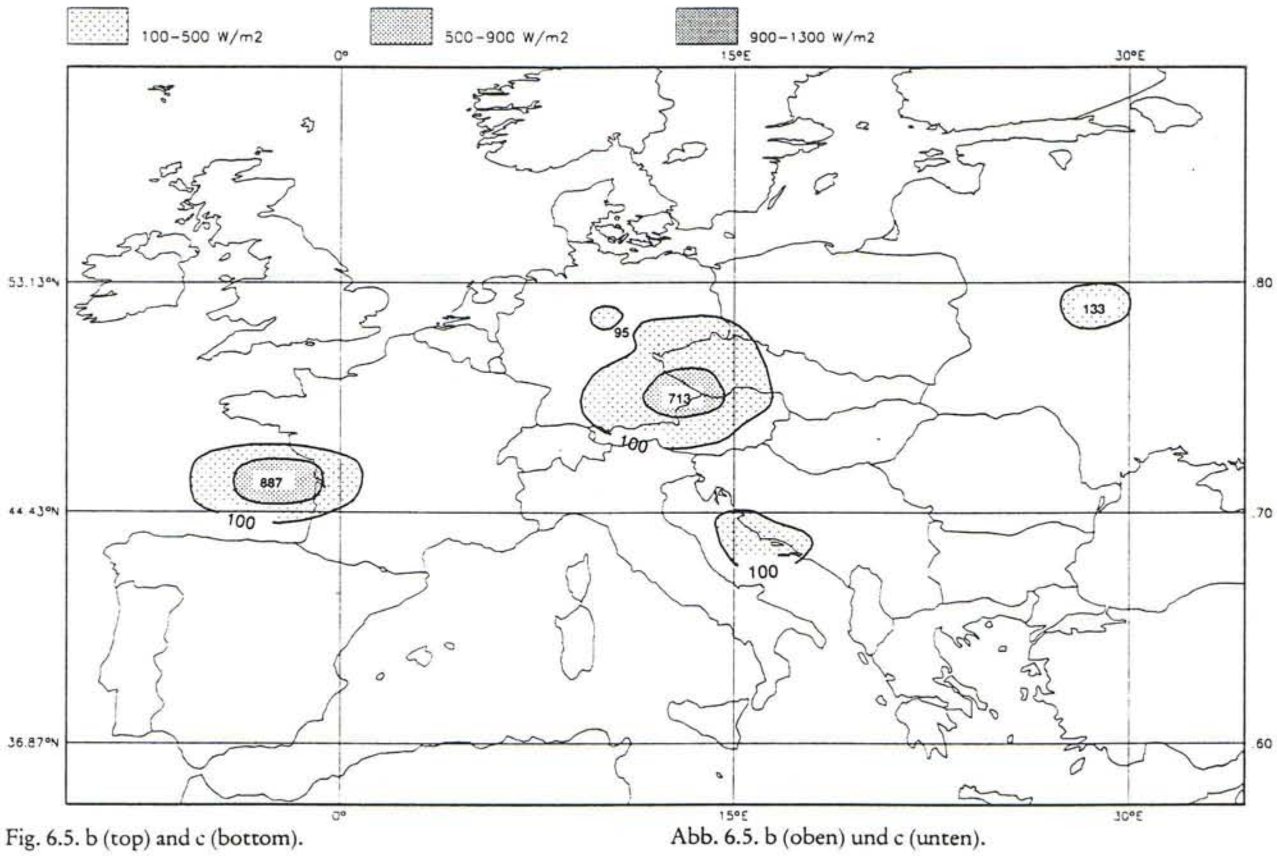

Fig. 6.5. b (top) and c (bottom).

Abb. 6.5. b (oben) und c (unten).

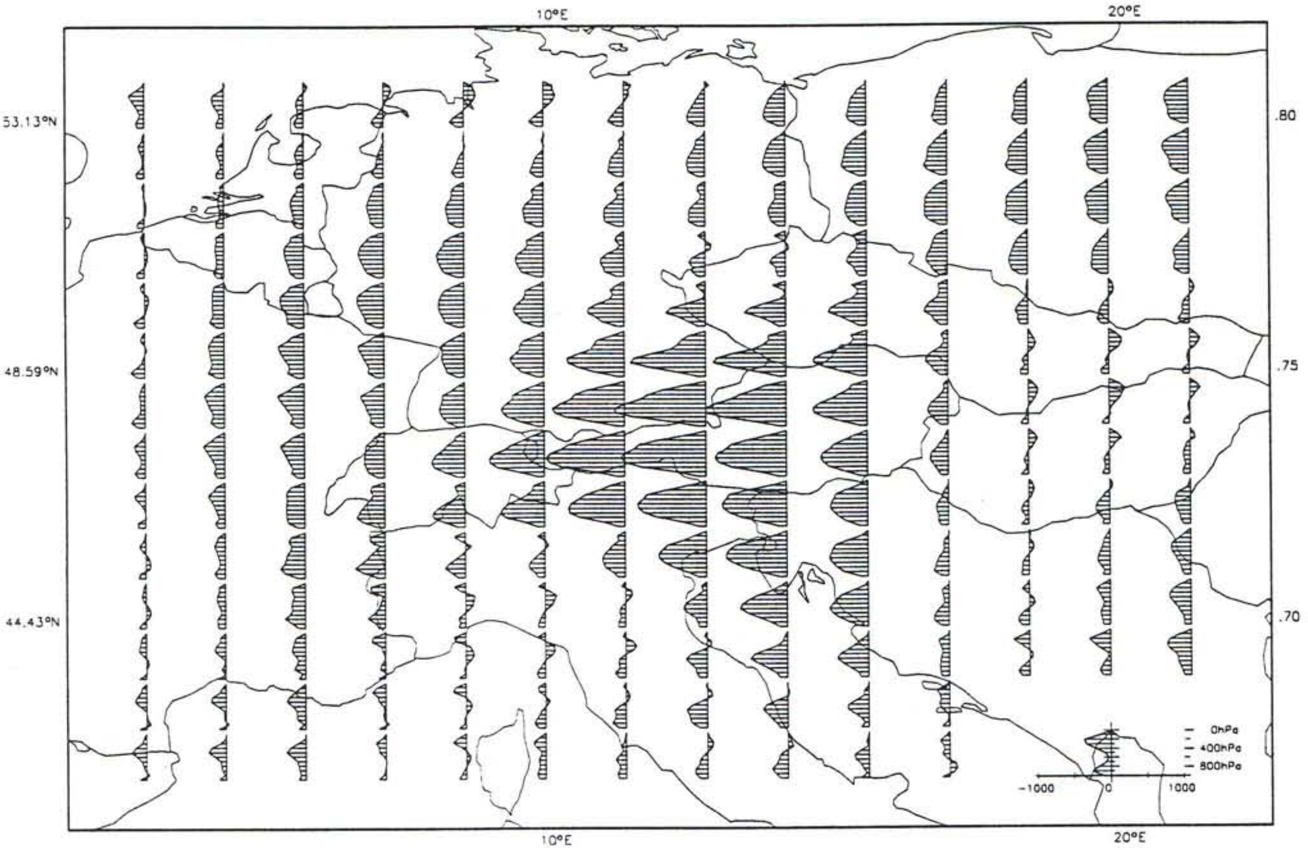

Fig. 6.6. Array of 14 × 14 diagnostic columns over Central Europe showing total convective heat flux h (= f + w) for 1 August 1991, 00GMT ± 6h, in units W/m² (compare Fig. 2.3); scale is indicated.

Abb. 6.6. Gesamtkonvektiver Wärmefluß h (= f + w) von 14 × 14 diagnostischen Säulen über Mitteleuropa vom 1. August 1991, 00GMT ± 6h, in W/m² (vgl. Abb. 2.3); Maßstab angegeben.

one objective measure could be the relative contribution of the sub-gridscale $\partial f/\partial p$ and of the gridscale b_q to $\partial r/\partial p$. According to Fig. 4.3, the maximum convergence of $\partial f/\partial p$ in the SALZBURG column on this day is —147 W/m² in the 600—700hPa-layer while b_q in the same layer amounts to —263 W/m²; neglecting the small imbalance of 18 W/m², these two together balance $\partial r/\partial p = 391$ W/m². This suggests that in this particular case about one third of the rain flux divergence can be explained by convection while two thirds can be attributed to the gridscale budget. This supports our understanding that the ECMWF forecast of the gridscale precipitation (Fig. 6.5b) is probably an underestimate, which may explain why the total forecast precipitation was off by a factor of about three.

To what extent this preliminary comparison may be representative remains a subject of further study.

7 Discussion and conclusions

This study is concerned with diagnosing the thermodynamic budgets of latent and sensible heat in the free atmosphere on the meso-beta scale over Europe. In its present first part we have described the implementation of a diagnostic model DIAMOD and its application to the August 1991 rain episode over Austria. The concept of this model has been the subject of various papers over the last decade. In its original form (HANTEL 1982, EMEIS & HANTEL 1984) the coupled budgets of latent heat and of dry static energy were studied in a coarse array of atmospheric boxes over the ALPEX domain. Each box measured (600 km)² in horizontal and 250 hPa in vertical direction, the time integration was over one day. The idea was to use the *observed* gridscale atmospheric fields (in analysed form) for an objective estimate of the *unobservable* sub-gridscale vertical fluxes. The divergences of these fluxes, determined as residuals from the gridscale quantities, are significant components of the thermodynamic budget equations. This approach is similar in many respects to the model of YANAI et al. (1973); it differs from the latter in the two important points that (i) YANAI's convection ensemble model is replaced through the more simple Bowen ratio closure assumption and (ii) that our diagnostic model yields an objective error estimate while YANAI's model does not.

One result of the original studies is reproduced in Fig. 7.1. It shows the sub-griscale fluxes r, f and w in an atmospheric column of the above dimensions centered over the Alps. Concerning w (labeled SH in Fig. 7.1) this flux consists not only of contributions of $T'\omega'$-eddies but also of $\Phi'\omega'$-eddies because HANTEL (1982) applied, instead of eq. (2.2)

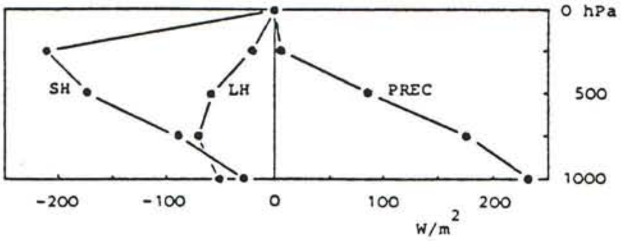

Fig. 7.1. Vertical profiles of r (labeled PREC), f (labeled LH) and w (labeled SH) for (600 km)² column over the Alps for pre-ALPEX day 19 January 1981 (HANTEL 1982); fluxes calculated for diagnostic boxes 250 hPa thick with preliminary version of DIAMOD.

Abb. 7.1. Vertikalprofile von r (bezeichnet mit PREC), f (bezeichnet mit LH) und w (bezeichnet mit SH) für (600 km)² Säule über den Alpen für Pre-ALPEX Tag 19. Jänner 1981 (HANTEL 1982); Flüsse mit Vorläuferversion von DIAMOD auf 250 hPa dicken diagnostischen Boxen berechnet.

above, the equation for dry static energy. The difference is however of no relevance for the present purpose because EMEIS (1985a, 1986) has suggested that the $\Phi'\omega'$-term is minor.

The original approach of this model as summarized by EMEIS & HANTEL (1984) has not much changed in the last decade. However, the quality of the thermodynamic model, of the data and of the resolution has considerably improved from 1982 to 1992. First, EMEIS (1985a) demonstrated that there is no reason to resort to the equation for the *dry static energy* c_pT+gz as a substitute for the *sensible heat* c_pT (or simply *heat* in the present paper). Actually, the sensible heat is thermodynamically more basic (it is the enthalpy of dry air) and its conservation equation does not explicitly require the hydrostatic assumption (as does the equation for dry static energy). Further, EMEIS showed that the results with the heat equation became more accurate than with the dry static energy equation. This made the model theoretically more consistent. HANTEL & EMEIS (1985) came up with a 156 km-resolution version of the model with rms-averages $imb_q = 68$ W/m² and $imb_T = 81$ W/m² and meteorologically consistent patterns of f and w. It was also demonstrated (HANTEL & EMEIS 1985) that in columns with convective precipitation the vertical sub-gridscale moisture flux can be much larger than the gridscale moisture flux.

The next step was to use improved data. They were provided by the finemesh analysis technique of REIMER (1980). Again for the ALPEX special observing period HANTEL (1987) presented a sequence of 5 consecutive daily averages of r, f and w; the accuracy was significantly higher (rms-imbalances of about 27 W/m² per diagnostic box).

With the established model it became possible to use this instrument for more detailed meteorological studies. BURKHARDT (1991), in an application of the diagnostic model to the African-Atlantic sector of the tropics (horizontal resolution about 250 km) found that the intertropical convergence zone (ITCZ) as defined by the maximum of convective activity and surface rain is not identical with the zone of maximum low level convergence; rather, the two are separated in meridional direction by a distance of 1000 km. BURKHARDT (1990, 1991) also showed that convective activity in the center of the ITCZ can be objectively defined by a maximum of upward directed f.

In order to apply DIAMOD for a deeper understanding of the physical processes in active weather zones we have tried in the present study to further improve the model quality, the input data quality and the space-time resolution. We shall briefly summarize first the merits and limits of the present implementation of DIAMOD and secondly the meteorological results that have emerged for the rain episode of August 1991.

7.1 *Conclusions for the implementation of DIAMOD*

The present implementation of DIAMOD uses the same set of equations that has already been employed by HANTEL (1987) or BURKHARDT (1990); this includes the horizontal discretization (3×3 gridpoints, arranged for equal area) and vertical discretization (10 pressure layers, 100 hPa each). In other words, there has not been any particular space discretization improvement of the theoretical model quality as compared to HANTEL (1987). However, the time discretization (3 time steps, now 6 hours apart) has been increased by a factor of two. The price for this improvement is that the imbalances have increased. DIAMOD yields the following output:

(a) A complete set of all diagnosed tendencies, flux divergences and fluxes, grid- and sub-gridscale of moisture and heat budgets, for each diagnostic box over the domain. Specifically, an imbalance is yielded for both budgets in each box which allows to objectively assess the overall quality of the overspecified atmospheric and surface input data. The rms-results for the rain episode studied are $imb_q = 42$ W/m² and $imb_T = 57$ W/m². These imbalances have increased as compared to HANTEL (1987) partly because the time resolution has been doubled and partly because the ECMWF analyses are diagnostically less consistent than were the data of REIMER (1980).

(b) When considered simultaneously, the imbalances can provide information which one of the input fields is more trustworthy than the other. For example, when imb_q and imb_T are equally large but of different sign this suggests that PREC may be dubious (too big when $imb_q < 0$ and too small when $imb_q > 0$). When imb_q is small but imb_T is large this suggests that the mass flux field may be erroneous, specifically the ω-field, while in the opposite case (large imb_q, small imb_T) the analysed moisture field may contain errors. Finally, when both imbalances are low which was the case in various representative areas of this study this allows for a detailed interpretation of the budget terms.

(c) The limits of the theoretical model as implemented in the present DIAMOD version will in a larger context be discussed in Part II of this study. They comprise the necessity of a closure assumption (*a priori* choice of a vertical inverse Bowen ratio profile), neglection of storage and horizontal transport of condensed material (including the constancy of L which actually should be temperature-dependent and allow for the distinction between water and ice), neglection of *horizontal* sub-gridscale moisture and heat fluxes and the neglection of any dissipation-dependent terms in the diabatic heating. Further, the vertical structure of the imbalances must be specified *a priori* and cannot be gained from any independent source. While all these shortcomings have without doubt a non-negligible quantitative impact upon the results it does not appear likely that by improving upon them DIAMOD will yield results that are qualitatively very much different; rather, the parameter that primarily limits the accuracy of DIAMOD's results is not the model itself but the input data.

(d) Concerning the synoptic input data quality we have used the analysed (not initialized) data as provided by ECMWF. While the analysis quality of the ECMWF data is excellent there is yet a problem. The ω-field is not analysed by the analysis procedure but is calculated from the horizontal velocity field by vertical integration; since the continuity equation is of first order, its solution can fulfill but one boundary condition. The consequence is that this ω is erroneous at the earth's surface (where it should be equal to the observed pressure tendency but actually is not). This state of affairs is further aggravated by the vertical interpolation to standard pressure surfaces in which form the data are provided by the data archive of ECMWF. In our implementation we have tried to make the wind field internally consistent by (i) specifying the observed surface pressure tendency for ω in the 1000 hPa-level and (ii) by applying our correction scheme which modifies all 3 mass flux components in every diagnostic box simultaneously for exact 3D-mass flux nondivergence (see WANG et al. 1992). The step (i) leads to a pronounced distortion of the mass-flux field close to the earth's surface which, even after application of step (ii), cannot be completely removed. A more consistent procedure would be to return to REIMER's (1980) method and combine step (i) with obtaining the ω-field from the ω-equation.

Why do we not use the *initialized* (instead of the *analysed*) data as provided by ECMWF, specifically in light of the fact that the analysed data still contain inconsistencies due to the ω-field? The answer is that in DIAMOD we do not try to maximize the consistency of the input data with a model but rather minimize the modifications to be applied to the observations.

(e) Concerning the surface precipitation we have employed an objective CRESSMAN analysis of the SYNOP data with a resolved scale that corresponds to the size of our diagnostic columns. There are severe limitations to improving this fairly rough analysis method due to the errors in the rain gauge measurements (e.g., SEVRUK 1985), to the limited representativeness of the station system and, finally, due to the anisotropy and non-homogeneity of the rain field characteristics.

(f) Concerning radiation and the surface fluxes other than rain we have as yet been satisfied with specifying a vertical radiation flux divergence which is constantly 10 W/m^2 per 100 hPa throughout the model domain. Likewise, we have used a constant $LH = -82\ W/m^2$ and a constant $SH = -17\ W/m^2$ over the model domain. While improvements in specifying the radiation flux divergence may be hard to achieve and will only be possible through heavy modeling, we expect that close-to-observed evaporation and sensible heat flux values at the surface, with realistic time and space variation, will further improve the accuracy of the input data; this will be one of the next planned implementations in DIAMOD.

(g) Concerning the space- and time-resolution of DIAMOD there is no point in pushing it much beyond the present value. As far as space is concerned, it may be doubtful that a, say, doubling of the horizontal resolution adds much to the analysis details of the ECMWF analyses (present status: T106L19), although this is speculation. As far as time is concerned, our present resolution of 12 hours is dictated by the rain gauge data which are available at no higher frequency; this applies to the operational net which, however, must remain to be the principal data source of DIAMOD.

(h) The present data set has, with DIAMOD, led to a sequence of results in which both the moisture and the heat budgets are characterized by: a budget of 50—120 W/m^2, a (slightly smaller) signal of 50—90 W/m^2 and a (considerably smaller) imbalance of 30—70 W/m^2. In other words, the imbalance, while not negligible, is consistently smaller than the signal (which itself is in many cases composed of relatively strong components that tend to cancel each other). Thus the fluxes calculated from the signal deserve credence.

7.2 Meteorological conclusions for the rain episode of August 1991

We now come to the meteorological results of this study. The synoptic situation was governed by a flat surface pressure distribution and a weak trough aloft with no pronounced frontal acitivity (Figs. 3.1, 3.2). As has been discussed in Section 6.2 the rain episode of the first August 1991 days over Central Europe was characterized by conditional instability of the precipitating air mass. This is also evidenced by Fig. 7.2. A vertical profile of equivalent potential temperature with its lower troposphere minimum is characteristic for moist unstable air masses in the tropics. While the station Wien is conditionally stable in Fig. 7.2 (and indeed experienced zero rainfall on 1 August) the station München was located in the tropical tongue which had been imported from the Mediterranean over Yugoslavia-Hungary. This air mass became most active on the northern fringe of the Alps and was eventually responsible for the precipitation maxima over Salzburg, Bavaria and Bohemia. The main results for this case as diagnosed with the aid of DIAMOD are as follows:

(a) The meteorological conditions during this episode supported excessive rain. We have considered (Section 4) the concentrated precipitation centered over Salzburg. In the column SALZBURG all components of the moisture budget (tendency, gridscale horizontal convergence, sub-

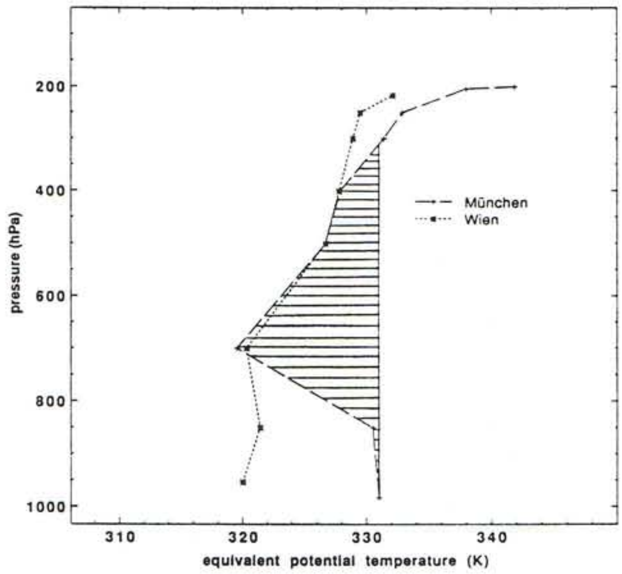

Fig. 7.2. Equivalent potential temperature for radiosonde stations Wien (moist stable — extratropical airmass) and München (moist unstable — tropical airmass) for 1 August 1991, 00GMT.

Abb. 7.2. Äquivalentpotentielle Temperatur aus Radiosondenaufstiegen über Wien (feuchtstabil-außertropische Luftmasse) und München (feuchtstabil-tropische Luftmasse) vom 1. August 1991, 00GMT.

gridscale vertical convergence) played together to maximize the surface rain. This mechanism peaked on 1 August.

(b) The total convective flux h = f + w (e.g., Fig. 6.6) is a quantity that can be diagnosed by DIAMOD with particular accuracy. It has been argued that h is quite insensitive to the model assumptions; this will be demonstrated in detail in Part II of this study (HANTEL et al. 1992). The pattern of h peaked over Austria on 1 August with values in the SALZBURG column exceeding 1000 W/m^2.

(c) Convection was however not the only mechanism active in the rain generation over Europe. 3D-gridscale moisture convergence was in an overall sense more relevant. With DIAMOD one can objectively differentiate between the two mechanisms. We have presented practically pure examples for either mechanism: the (moderate) rain in the column LJUBLJANA on 2 August was accompanied by sizeable convection but a vanishing moisture budget; on the other hand, the (relatively strong) rain in the column FREISTADT on 2 August was accompanied by a sizeable moisture budget but no convection.

(d) When there is convection but no rain this is recognized by DIAMOD. An example has been the column MILANO.

(e) In a preliminary comparison with ECMWF forecasts we have tried to demonstrate that a model-independent check of prognostic fields is possible with DIAMOD.

(f) How real are the vertical sub-gridscale fluxes, specifically the heat flux w? For example, is it possible that w is generated by a correlation between gridscale temperature and gridscale vertical velocity which simply is not resolved by DIAMOD's coarse boxes? If this were the case there should be a tendency that w becomes smaller with increased resolution. However, a comparison between Fig. 7.1 (resolution 600 km) and, for example, Fig. 4.1 (resolution 100 km) indicates that w tends to rise with increased resolution from 200 to more than 1000 W/m^2. This suggests that there must be eddy activity on scales far below the present resolved scale. Candidates are the cloud convective elements. Other eddy correlation mechanisms, not explicity resolvable on a routine basis, may be narrow frontal zones.

The diagnostic aspect of the present approach can be summarized in the remark that the amount of prejudices concerning the sub-gridscale effects is kept at a minimum in DIAMOD. This may be contrasted with the parameterization assumptions that are usually required in forecast models. The benefit of our intentional restriction is that we have been able to separate the convective flux from the rain flux in an objective manner. The application of this technique to various columns has yielded different budget types which have, in preliminary manner, been shown to be in accord with the meteorological conditions.

A *caveat*, already made in Section 6, may be repeated at the end. A budget and a discussion of its components, can never *explain* an observed property of the meteorological field in any complete sense. There is an infinite range of realizations available to the equations to cause the same rain at the ground. On the other hand, the results of the present study suggest that the budgets are not chaotically distributed. This is hardly a new finding but is consistent with established knowledge. Thus considering budgets remains to be a valuable and necessary (not sufficient) requirement for a complete understanding of atmospheric mechanisms. We have concentrated in the present paper upon the role of the sub-gridscale vertical fluxes of rain, moisture and heat. These are not the biggest, but hardly the least interesting and, up to now, somewhat neglected components of the moisture and heat budgets, at least as far as diagnostic studies are concerned.

It is clear that the eventual accuracy of the meteorological results as derived from DIAMOD is limited by the accuracy of the input data; diagnosed atmospheric data and observed surface precipitation cannot *a priori* fit together. However, DIAMOD is kept internally consistent due to the mass flux modification scheme. The remaining inconsistency of the data is comprised in the imbalances. This offers a chance to systematically reduce the imbalances through more accurate atmospheric plus surface data. Thus, DIAMOD may prove to be a valuable instrument in the arsenal of objective atmospheric analysis.

Acknowledgments

This study has been financially supported by the Austrian *Fonds zur Förderung der wissenschaftlichen Forschung*, Wien (Project P7330-GEO). The *European Centre for Medium-Range Weather Forecasts*, Reading, granted access to data and computer time within the Special Project "Subsynoptic vertical heat fluxes: comparison diagnosed vs modelled data". Cooperation with the *Zentralanstalt für Meteorologie und Geodynamik*, Wien, is acknowledged. The valuable comments of a reviewer are appreciated.

References

Bowen, I. S. (1926): The ratio of heat losses by conduction and by evaporation from any water surface. — Phys. Rev. **27**, 779—787.

Burkhardt, T. (1990): Subgrid-scale vertical heat fluxes over the African-Atlantic region. — Bonner Meteorol. Abh. **39**, 105 pp.

— (1991): Subgrid-scale vertical heat fluxes for the African region. — Meteorol. Atmos. Phys. **46**, 155—168.

Cressmann, G. P. (1959): An operational objective analysis system. — Month. Weath. Rev. **87**, 367—374.

Dorninger, M. (1992): Diagnose subskaliger Vertikalflüsse über Europa. — Diploma thesis at the University of Vienna (in German), 96 pp.

Emeis, S. (1985a): Subsynoptic vertical heat fluxes in the atmosphere over Europe. — Bonner Meteorol. Abh. **32**, 106 pp.

— (1985b): Kleinskalige Energietransporte in der freien Atmosphäre. — Geowiss. in unserer Zeit **3**, 181—186.

— (1986): Subsynoptic vertical energy fluxes in mid-latitude cyclones. — Meteorol. Rdsch. **39**, 161—172.

Emeis, S. & Hantel, M. (1984): ALPEX-Diagnostics: Subsynoptic heat fluxes. — Beitr. Phys. Atmos. **57**, 495—511.

Hantel, M. (1982): ALPEX: Subsynoptische Vertikaltransporte. — Ann. Meteorol. (N.F.) **19**, 79—80.

— (1986a): Variational modification of the 3D-wind field. — In: Variational Methods in the Geosciences, Y. Sasaki (ed.), Elsevier, 309 pp.

— (1986b): Rain in the free atmosphere from synoptic data. — Meteorol. Rdsch. **39**, 102—111.

— (1987): Subsynoptic vertical heat fluxes from high-resolution synoptic budgets. — Meteorol. Atmos. Phys. **36**, 24—44.

— (1989): Eine neue Gleichung für die atmosphärischen Energiehaushalte. — Wetter u. Leben **41**, 95—108.

Hantel, M. & Emeis, S. (1985): A diagnostic model for synoptic heat budgets. — Arch. Meteorol. Geophys. Bioklimat., Ser. A, **33**, 407—420.

Hantel, M., Reimer, E. & Speth, P. (1984): ALPEX-diagnostics: Quantitative synoptics over Europe. — Beitr. Phys. Atmos. **57**, 477—494.

Hantel, M., Ehrendorfer, M. & Haimberger, L. (1992): A thermodynamic diagnostic model for the atmosphere. Part II: The general theory and its consequences. — Manuscript in prep.

Holtslag, A. A. M. & Ulden A. P. van (1983): A simple scheme for daytime estimates of the surface fluxes from routine weather data. — J. Clim. Appl. Meteorol. **22**, 517—529.

Reimer, E. (1980): A test of objective meteorological analysis with optimum utilization of the radiosonde network in Central Europe. — Beitr. Phys. Atmos. **53**, 311—335.

Sevruk, B. (1985): Correction of precipitation measurements. — Zürcher Geogr. Schr. **23**, 288 pp.

Shao, Y. & Hantel, M. (1986): Subsynoptic vertical momentum flux in the atmosphere over Europe. — Bonner Meteorol. Abh. **33**, 159 pp.

Spangl, W. (1991): Skalige Budgets von Wärme- und Feuchtegleichung. Teil 1: Das Diagnostische Modell. — Unpubl. manuscript (in German), available from the authors, 88 pp.

Stull, R. B. (1988): An introduction to boundary layer meteorology. — Kluwer, 666 pp.

Wang, Y., Ehrendorfer, M. & Hantel, M. (1992): 3D-mass flux modification: Theory and numerics. — Manuscript in prep.

Yanai, M., Esbensen, S. K. & Chu, J. H. (1973): Determination of bulk properties of tropical cloud clusters from large-scale heat and moisture budgets. — J. Atmos. Sci. **30**, 611—627.

M. Dorninger
Dr. M. Ehrendorfer
Prof. Dr. M. Hantel
F. Rubel
Y. Wang
Institut für Meteorologie
und Geophysik
Universität Wien
Hohe Warte 38
A-1190 Wien

Received 12.11.1991, accepted: 28.11.1991